From the Department of Clinical Science, Intervention and Technology
Division of Radiology
Karolinska Institutet, Stockholm, Sweden

RADIOMICS IN CANCER PROGNOSIS: APPLICATIONS AND LIMITATIONS OF QUANTITATIVE TEXTURE ANALYSIS

Yi-Hua Zhang

Karolinska Institutet

Stockholm 2018

Cover image by Yi-Hua Zhang.
All previously published papers and figures were reproduced with permission from the respective publisher.
Published by Karolinska Institutet.
Printed by Universitetsservice US-AB.

ISBN 978-91-7831-266-5

Radiomics in cancer prognosis: Applications and limitations of quantitative texture analysis

THESIS FOR DOCTORAL DEGREE (Ph.D.)

By

Yi-Hua Zhang

Principal Supervisor:
Associate professor Torkel B. Brismar
Karolinska Institutet
Department of Clinical Science,
Intervention and Technology
Division of Radiology

Co-supervisor:
Ioannis Rouvelas M.D. Ph.D.
Karolinska Institutet
Department of Clinical Science,
Intervention and Technology
Division of Surgery

Opponent:
Associate professor Michael Torkzad
Royal Marsden Hospital,
UK & Telemedicine Clinic
Radiology Department

Examination Board:
Professor Anders Sundin
Uppsala University
Department of Surgical Sciences
Radiology

Professor Jarl Åsbjørn Jakobsen
University of Oslo
Institute of Clinical Medicine
Division of Radiology and Nuclear Medicine

Associate professor Jakob Hedberg
Uppsala University
Department of Surgical Sciences
Upper Abdominal Surgery

“If you just do your best, and believe in yourself, anything can happen.”

ABSTRACT

Medical imaging has become an integral part of clinical diagnostics since the discovery of X-rays at the end of the 19th century. Recent advances in computing power have opened up the possibility to extract quantitative data from medical images beyond what is visible to the human eye, so-called radiomics. Additional information from standard imaging modalities such as computed tomography (CT), magnetic resonance imaging (MRI), and positron emission tomography scan (PET) can thereby be acquired.

Texture analysis is one of the most studied methods within the concept of radiomics. The textural parameters calculated describe spatial relationships between voxel intensities and image heterogeneity. Methods based on gray level co-occurrence matrices (GLCM) are among the most common implementations of texture analysis of medical images. Recent studies have shown relationships between textural parameters and outcome parameters such as overall survival, treatment response and molecular markers in different types of cancers.

In this thesis, the potential application of textural analysis to be used as a prognostic tool in different cancers without requiring major changes to clinical imaging practice was evaluated.

In study I, a GLCM-based tool supporting analysis of 3D volumes was developed and applied for texture analysis of MRI images of low-grade glioma. The mutation status of isocitrate dehydrogenase (*IDH)* in low-grade glioma could be predicted using the GLCM textural parameter Homogeneity.

In study II, the use of semiautomatic segmentation was shown to reduce intra- and interobserver variation at CT volumetry of esophageal tumors when compared to manual segmentation. The influence of differing skill levels between the observers could also be reduced.

Study III showed that textural analysis could be used to predict ypT-status of post-neoadjuvant esophageal adenocarcinoma. Significant differences in textural parameters were observed between esophageal adenocarcinoma and squamous cell carcinoma, which suggest that the two tumor types should be analyzed separately in future studies involving textural analysis of esophageal cancer. The addition of PET image data during CT segmentation of esophageal tumors did not improve the correlation between the included textural parameters and ypT-status or overall survival.

Study IV found no additional variation in textural parameters due to use of contrast media for normal hepatic tissue or hepatic lesions, implying that reproducible contrast medium timing should not be an issue at perfusion CT texture analysis of hepatocellular carcinoma.

In conclusion, this thesis shows that histopathological differences in tumors can be observed using non-invasive diagnostic imaging through textural analysis. The method is applicable to both CT and MRI and on different types of tumors.

SAMMANFATTNING

Medicinsk bilddiagnostik har sedan upptäckten av röntgenstrålar i slutet av 1800-talet varit ett viktigt verktyg för klinisk diagnostik. Utvecklingen av datorberäkningskapacitet har möjliggjort tillämpningar av metoder för att beräkna kvantitativ data från medicinska bilder. Dessa tillämpningar ingår i samlingsbegreppet ”radiomics”, och har utvecklats som en ny källa för att få ut ytterligare information från vanliga bilddiagnostiska metoder som datortomografi (DT), magnetresonanstomografi (MRT) och positronsemissonstomografi (PET), utöver vad som kan uppfattas visuellt.

Texturanalys är en av de mest undersökta metoderna inom konceptet ”radiomics”. De texturparametrar som beräknas fram beskriver sambandet mellan intensitet mellan olika voxlar och kvantifierar visuellt uppfattade ojämnheter i bilder. Metoder baserade på beräkningen av matriser som beskriver samförekomst av gråskalor (gray level co-occurence matrices, GLCM) är bland de vanligaste tillämpningarna av texturanalys av medicinska bilder. Aktuella studier har påvisat samband mellan texturparametrar och utfallsmått som exempelvis överlevnad, behandlingsrespons och molekylära markörer för ett flertal cancerformer.

I denna avhandling undersöks om texturanalys, utan behov av förändringar av nuvarande rutiner för bilddiagnostik, kan tillämpas som prognostiskt verktyg för ett flertal cancertyper.

I studie I utvecklades ett GLCM-baserat verktyg för att analysera 3D volymer och användes för texturanalys av MRT bilder av låg-gradiga gliom. Genom beräkning av GLCM texturparametern Homogenitet kunde mutationsstatus av isocitratdehydrogenas (*IDH)* i låg-gradiga gliom förutsägas.

I studie II visades att användning av semiautomatisk segmentering, jämfört med manuell segmentering, minskade mätvariation inom och mellan observatörer vid DT volymetri av esofaguscancertumörer. Mätskillnad på grund av skillnader i erfarenhet mellan observatörerna kunde också reduceras.

Studie III visade att texturanalys kan användas för att förutsäga ypT-status i esofagalt adenocarcinom efter neoadjuvant behandling. Signifikanta skillnader i texturparametrar observerades mellan esofagalt adenocarcinom och skivepitelcancer, vilket medför att dessa tumörformer bör analyseras separat vid framtida studier av texturanalys av esofaguscancer. Tillägg av PET bilddata vid segmentering av DT bilder av esofagustumörer förbättrade inte korrelationen mellan de inkluderade texturparametrarna och ypT-status eller överlevnad.

I studie IV sågs ingen ytterligare variation av texturparametrar på grund av användning av kontrastmedel i normal levervävnad eller i lever lesioner. Detta tyder på att exakt reproducerbar tidpunkt av bildtagning vid användandet av kontrastmedel är av mindre vikt vid applikationer av texturanalys av perfusions-DT bilder av levercancer.

Sammanfattningsvis visar denna avhandling att histopatologiska skillnader i tumörer kan observeras med hjälp av icke-invasiv bilddiagnostik genom texturanalys. Metoden kan tillämpas på både DT- och MRT-bilder för flera typer av tumörer.

LIST OF SCIENTIFIC PAPERS

I. **Quantitative texture analysis in the prediction of IDH status in low-grade gliomas**
Jakola AS, Zhang Y-H, Skjulsvik AJ, Solheim O, Bø HK, Berntsen EM, Reinertsen I, Gulati S, Förander P, Brismar TB. *Clin Neurol Neurosurg. 2018 Jan;164:114–20.*

II. **Computed Tomography Volumetry of esophageal cancer - The role of Semiautomatic assessment**
Zhang Y-H, Fischer MA, Lehmann H, Johnsson Å, Rouvelas I, Herlin G, Lundell L, Brismar TB. *Submitted Manuscript, BMC medical Imaging*

III. **Texture analysis of computed tomography data using morphologic and metabolic delineation of esophageal cancer—relation to tumor type and neoadjuvant therapy response**
Zhang Y-H, Herlin G, Rouvelas I, Lundell L, Brismar TB. *Diseases of the Esophagus. 2018 Epub ahead of print*

IV. **Variation in textural parameters of hepatic lesions during contrast medium injection**
Zhang Y-H, Brehmer K, Svensson A, Herlin G, Stål P, Brismar TB. *Manuscript*

CONTENTS

LIST OF ABBREVIATIONS

AC	adenocarcinoma
AJCC	American Joint Committee on Cancer
AUC	area under the curve
BCLC	Barcelona Clinic Liver Cancer
CI	confindence interval
CT	computed tomography
EASL	European Association for the Study of the Liver
EUS	endoscopic ultrasound
FA	flip angle
FDG	fluorodeoxyglucose
FLAIR	fluid-attenuated inversion recovery
GLCM	gray level co-occurrence matrices
HCC	hepatocellular cancer
ICC	intraclass correlation coefficients
IDH	isocitrate dehydrogenase
*IDH*mut	*IDH* mutated variant
*IDH*wt	*IDH* wild-type variant
IQR	interquartile range
LGG	low-grade glioma
LQ	lower quartile
MELD	model for end-stage liver disease
ml	milliliter
mRECIST	modified Response Evaluation Criteria In Solid Tumors
MRI	magnetic resonance imaging
PCT	perfusion CT
PEI	percutaneous ethanol injection
PET	positron emission tomography
RANO	Response Assessment in Neuro-Oncology
RFA	radiofrequency ablation
ROC	receiver operating characteristic

ROI	region of interest
SCC	squamous cell carcinoma
SD	standard deviation
SUVmax	maximum standardized uptake values
TACE	transarterial chemoembolization
TARE	transarterial radioembolization
TE	Echo time
TI	inversion time
TR	repetition time
UICC	Union for International Cancer Control
UQ	upper quartile
US	ultrasound
ypT	post-neoadjuvant pathological tumor stage

1 INTRODUCTION

1.1 Low-Grade Glioma

Low-grade glioma (LGG) is a rare primary brain tumor, which predominantly occurs in relatively young patients between the late twenties to the mid-forties (1,2). The usual clinical manifestation is in the form of generalized tonic-clonic seizures, but a longer period of partial seizures for several months has also been observed (1,3). However, focal neurological signs are uncommon, as LGGs usually infiltrate brain parenchyma instead of compressing or destroying it. The use of diagnostic imaging in the form of magnetic resonance imaging (MRI) is an important part of diagnosing LGG but not recommended as the sole method (4). Histopathological analysis of surgical biopsy or resection is needed for final diagnosis (4,5).

The typical clinical course is relatively indolent compared to high-grade gliomas. However, there is a high level of clinical heterogeneity within LGGs and a clear connection between the molecular status of the tumor and overall prognosis has been identified (1,4). The isocitrate dehydrogenase (*IDH)* status (wild-type or mutated) and 1p-19q codeletion status are commonly used to stratify LGG; mutation of *IDH* and/or presence of 1p-19q codeletion are associated with prolonged overall survival (4,5). Although the morphologic appearance of *IDH* wild-type variant (*IDH*wt) is consistent with LGG from a molecular and clinical point of view, there are similarities to glioblastoma (6). However, the exact pathophysiological mechanism with which *IDH* mutations affects LGG prognosis is currently unknown. The prognostic significance of molecular status for LGG is reflected in the strong recommendation to test for *IDH* mutation and 1p-19q codeletion in the current 2016 WHO glioma classification guidelines (5) and that the molecular status supersedes cell morphology for the definition of tumor categorization. As *IDH* mutations are almost always found among tumors with 1p-19q codeletion, LGGs are usually categorized into those with *IDH* mutation and 1p-19q codeletion, those with *IDH* mutation but no 1p-19q codeletion and those with neither (5,6).

Current treatment strategies include long-term observation, surgery, radiation, and chemotherapy. However, the optimal management of LGGs is currently unclear. There are no clear indications that early surgery improves outcome in comparison to observation, and later intervention when detecting growth of the LGG (7). However, LGGs grow continuously, which renders the detection of growth and the need for future surgical intervention inevitable. The benefits of radiation and chemotherapy are currently unclear due to the lack of consensus regarding the timing and sequence of their usage. Current studies of radiation therapy have shown prolonged progression-free survival by 2 years, but no improvement of overall survival (8). Use of chemotherapy results in progression-free survival between 3 to 5 years (9). Recent findings also suggest that combining radiation with chemotherapy could improve survival (10) and a phase III trial, (ECOG-E3F05), comparing radiation therapy to chemoradiotherapy for high-risk LGG patients is currently ongoing (11).

1.1.1 Current role of diagnostic imaging

Diagnostic imaging in the form of MRI using a T2-fluid-attenuated inversion recovery (FLAIR) sequence is central in both the diagnosis and for assessing treatment response of LGGs. The use of MRI is preferred to computed tomography (CT) due to better delineation of the tumor and higher sensitivity to enhancement (12). The appearance is typically hypointense on T1-weighted sequences and hyperintense on T2-weighted and FLAIR sequences (Figure 1). Despite the observed clear margins on T2-FLAIR images, LGGs tend to infiltrate into surrounding tissue (13). There is usually little contrast enhancement, although up to 60% of LGG tend to have some enhancement of contrast. However, diagnostic imaging alone cannot be used for the staging of tumor grade, and histopathological examination of suspected tumor is required for the diagnosis and staging of LGG (4,5). MRI spectroscopy and positron emission tomography (PET) could potentially improve diagnosis but are not in routine clinical use (13–15).

Another role of diagnostic imaging is for long-term observation of LGG progression and assessing treatment response. The currently preferred method is MRI with a T2-FLAIR sequence, which offers information about tumor size and presence of peritumoral edema (12). As with diagnosis, use of MRI spectroscopy and positron emission tomography (PET) have been suggested in order to improve the reliability of the evaluation (16,17). However, the additional prognostic value is currently unclear. The Response Assessment in Neuro-Oncology (RANO) is the current guideline for assessing outcome in studies of LGG (18). The definitions of complete response, partial response and minor response to treatment are based on tumor size and appearance on T2-FLAIR MRI images, thus highlighting the role of diagnostic imaging in response assessment.

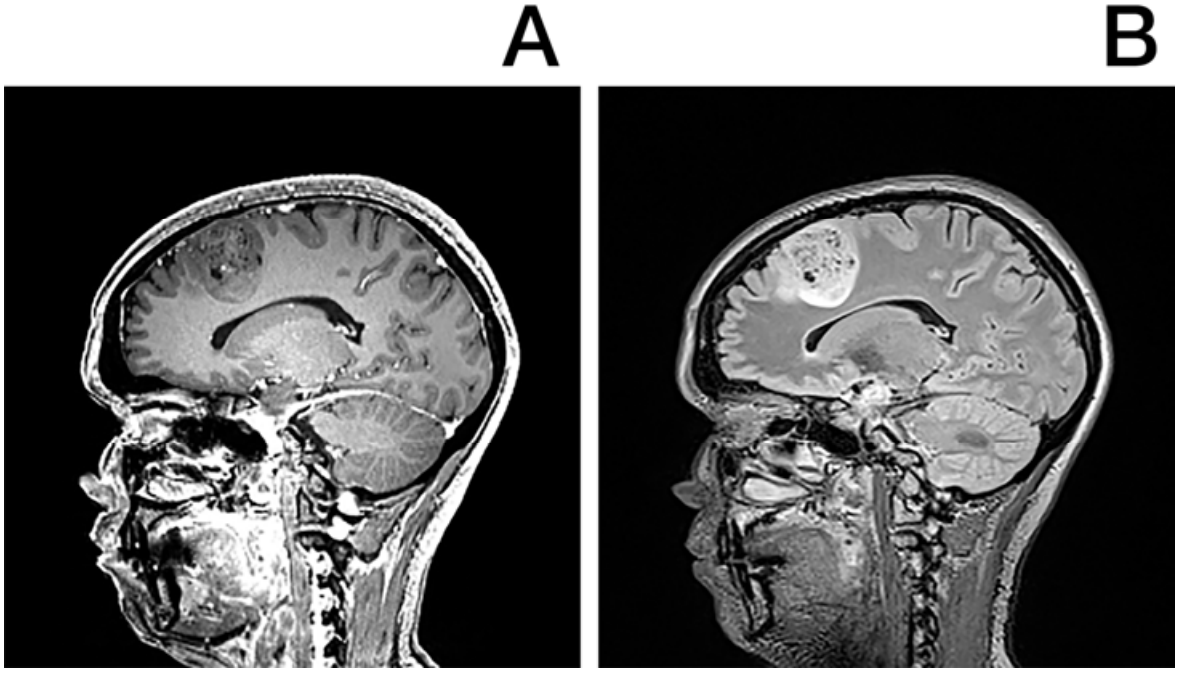

Figure 1 *Magnetic resonance images of low-grade glioma on T1-weighted (A) and T2-weighted FLAIR (B) images.*

1.2 Esophageal Cancer

Esophageal cancer is a common cancer form in the world and the sixth most common cause of cancer death. The two major histological types are squamous cell carcinoma (SCC) and adenocarcinoma (AC) (19–22). SCC is more common globally, but AC is more common in Western populations, which is attributed to obesity and high prevalence of gastroesophageal reflux (23,24). Clinical presentation is asymptomatic during the early stages; more advanced disease usually presents with progressive dysphagia, with difficulty of swallowing solids initially and followed by liquids as the disease progresses. Unintentional weight loss is also commonly observed (25). Overall 5-year survival is currently around 25%. The lack of symptoms until later advanced stages of the disease results in only 25% being eligible for curative therapy due to delay of diagnosis (20–22). Endoscopic examination of the esophagus and stomach with biopsy of suspicious lesions is currently the preferred method for initial diagnosis. Later staging is a multi-modal process involving endoscopic ultrasound (EUS), CT and fluorodeoxyglucose (FDG)-PET in order to asses tumor size (T-stage), evaluate lymph node status (N-stage) and screen for metastases (M-stage) (19,20,26).

Current treatment options depend on the histological type of esophageal cancer. However, most patients treated with curative intent undergo neoadjuvant chemotherapy or chemoradiotherapy in combination with surgical resection management (27). For SCC, the use of only chemoradiotherapy has been shown to be a possible option management (27). The difference in prognosis and treatment response between AC and SCC has recently given rise to the viewpoint that they are different unique diseases and need different clinical management (27). The assessment of treatment response after neoadjuvant treatment is based on grading histopathological tumor tissue response as there is no reliable noninvasive method or prognostic biomarkers for response assessment (28). The agreement of tumor tissue response between endoscopic biopsy and the final resected tumor is not good enough to base the treatment strategy on biopsy (29). This is probably due to sampling errors caused by uneven distribution of tumor response and ingrowth of fibrotic tissue (28). Furthermore, assessment using endoscopy and endoscopic ultrasound is not always possible due to local inflammation and strictures following neoadjuvant therapy (30). They are also invasive procedures associated with patient discomfort and potential iatrogenic risk.

1.2.1 Current role of diagnostic imaging

The primary use of diagnostic imaging in the management of esophageal cancer is to stage newly diagnosed tumors after initial endoscopy through assessment of tumor size, size of local lymph nodes and to screen for metastases (19,20,26). The preferred modalities are CT for evaluation of locoregional status and FDG-PET to screen for distant metastases. Combined FDG-PET/CT is often used when available (19,20,26). Studies assessing neoadjuvant treatment response using diagnostic imaging have focused on CT and PET images and assessment of tumor volume, or PET-specific parameters such as maximum standardized uptake values (SUVmax) (31–33). Measured parameters of both pre- and post-neoadjuvant therapy examinations have been analyzed but different conclusions have been reached (31–33). The clinical and research value is therefore still controversial.

1.3 Hepatocellular Cancer

Hepatocellular cancer (HCC) is a very common cancer form, causing the second most cancer-related deaths globally (34). It is also estimated to cause the greatest health-related economic cost worldwide (34). Risk factors for HCC include causes of liver cirrhosis, such as hepatitis B or C infection, alcohol consumption, nonalcoholic steatohepatitis, biliary cirrhosis, genetic factors etc (35). Non-cirrhosis related risk factors are being a carrier of hepatitis B or C virus. Clinical presentation is usually asymptomatic until advanced disease, where typical symptoms are weight loss and pain in the upper right quadrant (36). Among patients with known liver cirrhosis, HCC can manifest as sudden hepatic decompensation (36). Screening programs of high-risk populations such as patients with chronic viral hepatitis or cirrhosis have been implemented in order to diagnose HCC at an earlier stage in order to enable the use of potentially curative treatment options. These screening programs monitor levels of alpha-fetoprotein and use diagnostic imaging methods such as ultrasound (US), multiphase contrast-enhanced CT and contrast-enhanced MRI (37–39).

Usually, only diagnostic imaging is needed for the diagnosis of typical HCC lesions in patients with liver cirrhosis (39,40). Biopsy is only needed when the appearance of the lesion is nontypical on CT or MRI or in patients with a non-cirrhotic liver (39,40). Staging of HCC in Europe is usually performed according to the Barcelona Clinic Liver Cancer (BCLC) staging system, which takes into account the tumor stage, liver function and physical status (39,41). Liver function is commonly assessed using either the Child-Pugh classification (42,43) or the model for end-stage liver disease (MELD) (44).

There are currently several options for treatment of HCC, although only surgical resection, liver transplantation, and ablation are considered curative treatments, where the choice of method depends on the number of lesions and the presence of cirrhosis (45). Surgical resection is the preferred method when only a single lesion between 2-5 cm in size is present, while liver transplantation is indicated for patients with either a single lesion < 5 cm or up to three lesions, each smaller than 3 cm in size (39,40). Ablation using percutaneous ethanol injection (PEI) or radiofrequency ablation (RFA) is used when the patient is not eligible for surgical treatment (39,40). However, diagnosis of HCC is often made at a late stage where no effective treatment is available (46). Treatment options for those cases are transarterial chemoembolization (TACE), where the arterial blood supply of the HCC is cut off using embolization of supplying arteries, transarterial radioembolization (TARE), where radioactive microspheres are directed into the tumor using a catheter and systemic therapy using Sorafenib (39,40).

1.3.1 Current role of diagnostic imaging

The role of diagnostic imaging for HCC is extensive, including screening, diagnosis, and evaluation of treatment response (39,40,47). Screening of high-risk patients is usually done using US at regular intervals, with additional examinations using multiphase contrast-enhanced CT, perfusion CT (PCT) and contrast-enhanced MRI when needed (37–39). HCC lesions have a typical appearance with contrast uptake in the arterial phase followed by washout of contrast in the late venous phase (Figure 2) (35,48). Further investigation using needle biopsy is usually not required (39,40). Treatment response of HCC is usually measured using a modification of the Response Evaluation Criteria In Solid Tumors (mRECIST) guidelines (40).

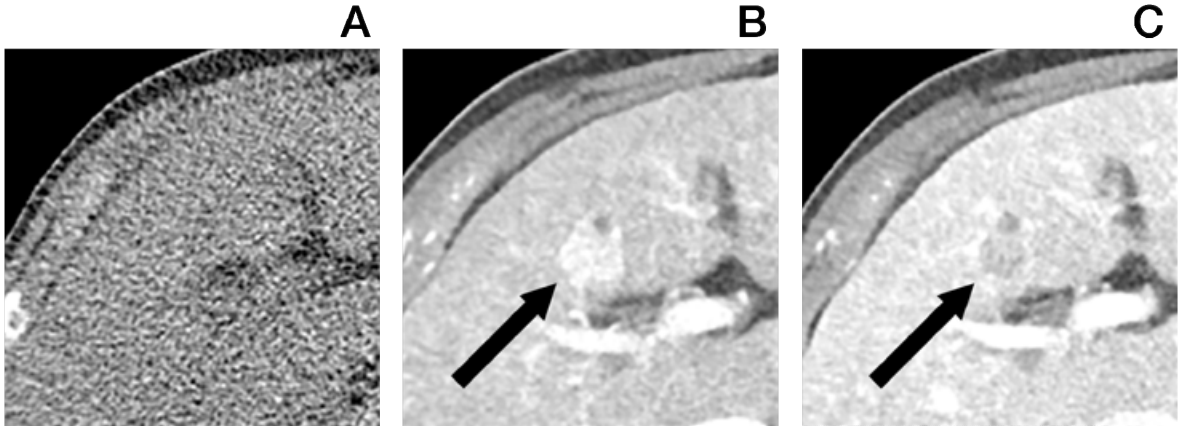

Figure 2 *Computed tomography images of a hepatocellular cancer lesion in native (A), arterial (B) and portal-venous (C) contrast phase. Typical contrast uptake in the arterial phase followed by contrast washout in the lesion can be observed.*

1.4 Texture Analysis

Texture analysis refers to a set of methods for quantitative image processing used to characterize spatial relationships between voxel intensities. This enables the calculation of quantifiable parameters to describe visually perceived image heterogeneity. Textural analysis parameters are also commonly included in the concept of radiomics, often in combination with related parameters describing shapes and intensity (49). Although the methods used to calculate textural parameters have been known for decades, only recent advances in computing power have made them feasible to implement in clinical practice. This has enabled several recent studies evaluating the relationship between textural parameters and outcome parameters such as overall survival, treatment response and molecular markers in different types of cancers (50–53). Earlier studies have often been limited to analysis of a single 2D slice (54–57), but more recent studies have also extended the analysis into 3D (58,59). The quantified heterogeneity is currently interpreted to be correlated to tumor heterogeneity and reflect tumoral microangiogenesis, necrosis, hypoxia, metabolism and other parameters of tumor microbiology (60–63). However, no conclusive biological explanation for the image heterogeneity of tumors is currently available.

1.4.1 Segmentation of volumes of interest

Use of texture analysis requires segmentation of the volumes of interest to be used for processing. Earlier studies have applied manual segmentation where the tumor is manually delineated on all image slices where it is visible, which is a time-consuming process and suffers from high intra- and interobserver variability (64–66). Advances in computing power have enabled the development of several methods for automating parts of that procedure. The development of semiautomated methods reduced the number of slices in a tumor needing human delineation from every slice to only some of the slices by interpolating the segmentation of the rest of the slices (67,68). The resulting segmented tumor volume can then be corrected by minor manual adjustments. Later, more advanced automated methods that only require the tumor to be highlighted where the segmentation of the rest of the volume is then automatically completed have been presented (59,69). The most advanced methods allow localization and volume segmentation to be done with little or no human input (70–72).

1.4.2 Gray level co-occurrence matrices

Several methods are available for calculation of textural analysis parameters; some of the most commonly used are based on gray level co-occurrence matrices (GLCM) (49,52). These are generated through the frequency of adjacent voxel intensities, which are found together at a certain offset direction. The matrices are then calculated for each offset and are used for the calculation of the textural parameter chosen for use. Some offsets are just mirrored variations of other offsets and add no additional information when included in the calculation of the textural parameters. For 2D images the resulting matrices for 0 and 180 degrees offset, 45 and 135 degrees, 90 and 270 degrees and 135 and 315 degrees are identical, thus calculation of

only four matrices are required to consider all potential directions of offset in 2D images. For 3D images, 13 matrices are required (73,74).

In the paper first describing this method by Haralick there were 28 parameters included (73). Further work by Conner et al. reduced the number of parameters of interest to seven, as several of the described parameters were considered redundant (75). The remaining parameters are Energy, Entropy, Correlation, Inverse difference moment or Homogeneity, Inertia or Contrast, Cluster Shade, and Cluster Prominence. In this thesis, the parameters Energy, Entropy, Correlation, Homogeneity, and Inertia were selected for further use, as they were better studied in literature at the time the included studies were planned. The parameters can be divided into those that highlight differences between adjacent voxels (Inertia and Homogeneity), those that highlight the regularity of the differences in the image (Energy and Entropy) and the one that describes the relationship of the differences in the image (Correlation) (74).

Higher levels of heterogeneity in an image usually result in higher values of Inertia and Entropy, and lower values of Homogeneity, Energy, and Correlation. Example images resulting in high and low values of textural parameters are shown in Figure 3.

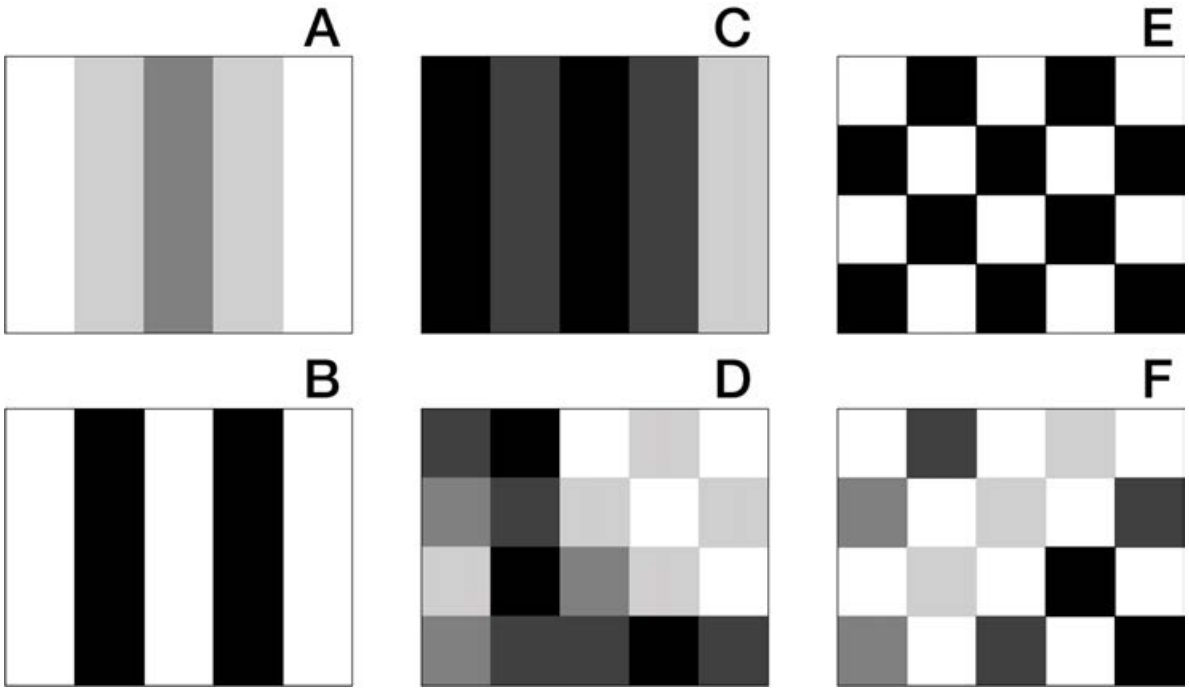

Figure 3 *Example images resulting in high and low values of textural parameters calculated from gray level co-occurrence matrices according to the formula described by Haralick. Image A and B differ in the differences between pixel values, thus resulting in low Inertia and high Homogeneity for A and vice versa for B. Image C and D differ in the regularity of pixel value changes, which results in high Energy and low Entropy for Image C and vice versa for Image D. Image E and F differ in the amount of pixel value change between the white pixels and the colored pixels. This results in high Correlation for image E and low for image F.*

1.4.3 Other methods of texture analysis

Fractal analysis refers to a set of methods used to calculate the fractal dimension of the analyzed image data. The calculated fractal dimension represents information about the shape and complexity of the analyzed image and this value is then used as the parameter for comparison. Currently, fractal analysis has been used for analysis of brain imaging, mammography, and bone imaging. Potential advantages in comparison to GLCM texture analysis is lower computation cost, but few studies assessing this set of methods are available (49,76,77).

Filters and transformations are methods to process specific areas of the image. The extracted value represents a certain spatial feature depending on the type of filter used, which is used for further analysis (78). Filters and transformation can also be used as a pre-processing step before further analysis using other methods, for example by using a Laplacian of Gaussian transformation to extract image features of a certain size before. This technique is for instance used by the commercial TexRAD texture analysis software (TexRAD, Cambridge Computing Ltd, UK) (51).

1.4.4 Potential clinical applications of texture analysis

The proposed correlation of texture analysis and tumor heterogeneity have resulted in several studies of the use of texture analysis to predict tumor prognosis, tumor treatment response and tumor identification (49,52,54,79,80). The quantifiable nature of the parameters enables computer processing of qualitative image features such as the degree of disorder, irregularity of shape, spiculation etc, which could potentially enable a higher degree of automation. Combining texture parameters with other radiomic features could improve tumor characterization and offer currently unavailable prognostic information.

1.4.4.1 Low-Grade Glioma

Previous studies have shown promising applications of radiomics combined with machine learning in order to provide prognostic information in high-grade glioma patients (81–84). The use of radiomics on a combination of metabolic MRI and anatomic MRI has been shown to predict the molecular status of high-grade gliomas and thus offer non-invasive prognostic information (85). It has also been shown that radiomics of MRI can be used to differentiate high-grade glioma from LGG (86) and be used to predict *IDH* status when combined with deep learning (87). This suggests that texture analysis of LGG could have potential applications in the prediction of molecular status through analysis of MRI images and offer non-invasive prognostic information for LGG patients.

1.4.4.2 Esophageal Cancer

Recent studies of radiomic parameters of CT and PET images of esophageal carcinomas have shown to offer prognostic value in predicting survival and neoadjuvant treatment response (53). On PET images, the examined radiomic parameters offer additional information on treatment response in comparison to conventional PET parameters such as SUVmax and metabolic tumor volume (88–90). Higher levels of calculated tumor heterogeneity have been shown to have worse prognosis (55–58). The most common significant radiomic feature was GLCM Entropy, which highlights the potential prognostic value of texture analysis for treatment response assessment. Similar studies of CT images have shown similar results, with worse outcome for tumors with higher heterogeneity (53).

Current radiomic studies of esophageal carcinoma have often analyzed AC and SCC together (53). The histological differences between these cancer types and clinical observations regarding differences in clinical behavior and treatment response between AC and SCC have led to the viewpoint that they are different diseases (27). As textural parameters are assumed to reflect tumor microbiology, separate texture analysis of AC and SCC could potentially reveal differences in textural parameters between these tumor types, which would have to be considered for future applications of radiomics of esophageal carcinoma.

1.4.4.3 Hepatocellular Cancer

Radiomic parameters have been shown to correlate with molecular parameters and treatment response in HCC (51,91,92). Quantified image heterogeneity in HCC has shown prognostic information on the outcome after surgical resection where those with higher heterogeneity at CT imaging had worse prognosis than those with lower (91). This highlights a potential use of texture analysis for identifying cases where alternative treatments might be tested. In addition, they can be used to quantify the degree of liver steatosis, fibrosis, and cirrhosis (93–95).

At US and MRI elastography, the parameter stiffness is used to diagnose and grade liver fibrosis (96,97). Texture analysis could potentially offer a principally different method of measurement, as it is not believed to measure stiffness (93–95). This would also reduce the number of different diagnostic procedures for the patients as they often undergo CT scans for other reasons.

The altered blood supply in HCC compared to that of normal liver parenchyma results in its observed typical contrast dynamics during contrast injection with high contrast enhancement in the arterial phase and a washout in the late venous phase (35,48). When applying texture analysis on HCC the timing of image acquisition can potentially affect the measured textural parameters. The variation in textural parameters during contrast medium injection in HCC and the importance of precise timing has to our knowledge not been elucidated previously.

1.4.5 Challenges regarding implementation of texture analysis

Current challenges regarding the implementation of texture analysis are associated with the sensitivity to minute changes of image data that might be hard to detect using the human eye. Use of different scanners and image acquisition settings affects the resulting image and analysis (98,99). Contrast enhancement could introduce further variation both in comparison to unenhanced images and during the contrast injection. This is explored further in study III and IV of this thesis. The process of segmentation is also a source of variation and can also be too time-consuming to use in clinical practice. The reproducibility of segmentation is examined in study II. The selection of textural parameters can lead to redundancy due to positive correlation between the selected parameters. Some parameters also show volume dependence, which has to be considered during statistical analysis (49). Radiomic applications also tend to lead to a very high number of extracted features, which are then used for analysis on small populations, leading to false positive results (49,89). Due to all these factors, reproducibility of studies of textural parameters can be challenging as many factors need to match to enable comparison between studies.

2 AIMS

The aim of this thesis was to evaluate the potential application of textural analysis to be used as a prognostic tool in different cancers without requiring major changes to clinical imaging practice.

Specific objectives of each study were:

Study I

To implement a GLCM-based texture analysis tool supporting analysis of volumes of interest from MRI and to assess its prognostic value for low-grade glioma.

Study II

To evaluate whether the use of semiautomatic segmentation can reduce interobserver variation at esophageal cancer segmentation.

Study III

To examine the prognostic value of textural analysis for esophageal cancer and to investigate the association between textural parameters derived from CT image data and histopathological characteristics.

To study whether the refinement of tumor volume segmentation of esophageal cancer through the addition of PET image data can further improve the prognostic value of textural parameters.

Study IV

To study HCC textural parameters during contrast medium injection in order to quantify and compare the variation of textural parameters over time between different HCC lesions and normal hepatic parenchyma. To evaluate whether the timing of the image acquisition during contrast medium injection is important for obtaining reproducible measurements of textural parameters.

3 METHODS

3.1 Study population

3.1.1 Low-Grade Glioma

Study I. A total of 25 patients with newly diagnosed diffuse LGG treated at St. Olavs hospital (Trondheim, Norway) were recruited during 2008-2016 for this retrospective study. Included patients had histopathologically verified supratentorial LGG and preoperative 3T digital images from a Siemens Skyra MRI scanner (Siemens, Erlangen, Germany) between 2008 and 2016. End of follow-up was 2016-01-01. Radiological and clinical data were retrieved from medical journals and previous research projects. Further patient details are shown in Table 1.

Status of *IDH* mutation and 1p-19q codeletion were analyzed according to a previously described method (100).

Table 1 *Patient, treatment and tumor characteristics for low-grade glioma patients.*

	n=25
Age, mean (SD)	44 years (14)
Gender (M:F)	16 (64%): 9 (36%)
Seizure	15 (60%)
Resection	25 (100%)
Histopathology	
Astrocytoma *IDH*wt	5 (20%)
Astrocytoma *IDH*mut	9 (36%)
Oligodendroglioma	11 (44%)
Radiotherapy	
After primary surgery	2 (8%)
After redo surgery	8 (33%)
Missing	1
Chemotherapy	
Upfront	0
At progression/transformation	8 (33%)
Missing	1
Later tumor resection	10 (40%)
Progression during follow-up	10 (40%)
Malignant transformation during follow-up	8 (32%)
Significant contrast enhancement	1 (4%)
Verified with histopathology	7 (28%)
Deceased during follow-up	3 (12%)

3.1.2 Esophageal Cancer

The patients included in study II and III were previously included in a multicenter randomized clinical trial comparing two neoadjuvant regimens for a study cohort of 181 esophageal cancer patients, 131 adenocarcinomas and 50 squamous cell carcinomas (101). The patients were recruited during 2006–2012 and had histologically confirmed adenocarcinoma or squamous cell carcinoma of the esophagus or gastroesophageal junction. Clinical tumor stage at inclusion was T1-3, any N except T1N0, and all patients were eligible for curative treatment with surgical resection when included. Tumor histology was verified through histological typing of the surgically resected tumor or multiple endoscopic biopsies if the patient was not applicable for surgical treatment due to disease progression during neoadjuvant treatment. Patients were evaluated clinically and radiologically before and after three cycles of induction chemotherapy with cisplatin and 5-fluorouracil or three cycles of chemotherapy with cisplatin and 5-fluorouracil combined with 40 Gy radiotherapy in preparation for curative resections. Patients not eligible for curative treatment, having concomitant malignancy, complications of diabetes or uncontrolled cardiac disease were excluded from the trial.

Study II. Inclusion criteria for this retrospective sub-study were the availability of baseline spiral CT for tumor staging from our clinic before the start of neoadjuvant treatment with the presence of scans with 0.625mm slices from both arterial and portal-venous phase. Patients with metastatic diseases or subject to endoscopic stent placement or other treatment prior to the CT scan were excluded. A subset of 23 esophageal cancer patients was included (median age 65, range 51-71). Detailed individual patient characteristics are shown in Table 2.

Table 2 *Details about patients (n=23) included for the manual segmentation and semiautomatic measurements. AC = Adenocarcinoma, SCC Squamous cell carcinoma, SI = Siewert I, SII = Siewert II.*

	Sex	Age	BMI	Cancer Type	TNM Stage	Tumor Location	Neoadjuvant Therapy	Resected
1	M	71	22	SCC	T2N1M0	Middle	Chemoradiotherapy	Yes
2	F	70	25	AC	T3N1M0	Cardia, SII	Chemoradiotherapy	Yes
3	M	69	25	AC	T2N0M0	Distal	Chemoradiotherapy	No
4	M	67	24	AC	T3N1M0	Cardia, SII	Chemotherapy	Yes
5	M	69	24	AC	T3N1M0	Cardia, SII	Chemotherapy	Yes
6	M	63	22	SCC	T3N1M0	Middle	Chemotherapy	Yes
7	M	64	22	SCC	T3N1M0	Middle	Chemotherapy	Yes
8	M	64	30	AC	T3N1M0	Distal	Chemoradiotherapy	Yes
9	M	67	22	AC	T3N0M0	Cardia	Chemoradiotherapy	No
10	M	66	27	SCC	T3N1M0	Middle	Chemoradiotherapy	Yes
11	M	68	24	AC	T3N1M0	Distal	Chemotherapy	Yes
12	M	65	32	SCC	T3N1M0	Distal	Chemotherapy	Yes
13	M	63	33	AC	T3N1M0	Cardia, SII	Chemoradiotherapy	Yes
14	M	62	25	AC	T2N0M0	Cardia, SI	Chemotherapy	Yes
15	M	63	28	AC	T3N1M0	Cardia, SII	Chemotherapy	Yes
16	M	60	23	SCC	T2N1M0	Middle	Chemoradiotherapy	Yes
17	M	61	30	AC	T3N0M0	Cardia, SII	Chemoradiotherapy	Yes
18	M	58	21	SCC	T3N1M0	Distal	Chemotherapy	No
19	F	56	22	SCC	T3N1MX	Distal	Chemoradiotherapy	Yes
20	M	56	34	AC	T2N0M0	Cardia, SII	Chemotherapy	Yes
21	M	57	26	AC	T3N0M0	Cardia, SII	Chemoradiotherapy	Yes
22	F	52	20	AC	T3N1M0	Cardia, SII	Chemoradiotherapy	Yes
23	M	51	23	AC	T3N0M0	Cardia, SII	Chemoradiotherapy	Yes

Study III. Inclusion criteria for this retrospective sub-study was that spiral CT in the portal-venous phase and PET/CT investigations had been completed at our clinic with 1.5mm slices before and after neoadjuvant treatment and that the patients had been admitted to Karolinska University Hospital, Sweden. Patients with PET/CT examinations from other clinics, with different slice thicknesses, or receiving esophageal stents during treatment were excluded.

A subset of 36 esophageal cancer patients was included in the study. After neoadjuvant treatment, all 36 patients underwent surgical resection and histopathological data from the tumors was obtained. Of the analyzed tumors, 11 were squamous cell carcinoma and 25 adenocarcinomas. Details of the included patients are shown in Table 3.

Table 3 *Characteristics of the 36 patients included in the study divided into Adenocarcinoma and Squamous Cell carcinoma subgroups.*

	Adenocarcinoma (n = 25)	**Squamous cell carcinoma (n = 11)**
Median age	64 years (range 50–75)	62 years (range 45–73)
Gender (M:F)	19 (76%): 4 (16%)	10 (91%): 1 (9%)
Median body weight	83 kg (range 51.6–119)	74 kg (range 63–122)
BMI	26.4 (range 20.2–34.0)	25.0 (range 20.3–33.4)
Tumor location		
Esophagus	3 (12%)	11 (100%)
Upper third	0 (0%)	1 (9%)
Middle third	1 (33%)	7 (64%)
Lower third	2 (67%)	3 (27%)
Junction	22 (88%)	0 (0%)
Siewert I/II/III	3 (14%) / 19 (86%) / 0 (0%)	
Clinical T stage		
cT1/cT2/ cT3/cT4	0 (0%)/6 (24%)/ 19 (76%)/0 (0%)	0 (0%)/4 (36%)/ 7 (64%)/0 (0%)
Clinical N stage		
cN0/cN1/ cN2/cN3	8 (32%)/16 (64%)/ 1 (4%)/0 (0%)	2 (18%)/9 (82%)/ 0 (0%)/0 (0%)
Clinical M stage		
cMX/cM0/cM1	1 (4%)/23 (92%)/1 (4%)	1 (9%)/10 (91%)/0 (0%)
Clinical Stage		
Stage 0/1/ 2/3/4	23 (92%)/0 (0%)/ 0 (0%)/2 (8%)/0 (0%)	9 (82%)/0 (0%)/ 1 (9%)/1 (9%)/0 (0%)
Neoadjuvant Pathological T stage		
ypT0/ypTis/ypT1/ ypT2/ ypT3/ypT4	2 (8%)/1 (4%)/4 (16%)/ 3 (12%)/13 (452%)/2 (8%)	3 (27%)/0 (0%)/0 (0%)/ 4 (36%)/4 (36%)/0 (0%)
Neoadjuvant Pathological N stage		
ypN0/ypN1/ ypN2/ypN3	9 (31%)/6 (24%)/ 5 (20%)/5 (20%)	8 (73%)/1 (9%)/ 2 (18%)/0 (0%)
Neoadjuvant therapy		
Chemotherapy	12 (48%)	5 (45%)
Chemoradiotherapy	13 (52%)	6 (55%)
Overall survival		
Alive	9 (36%)	3 (27%)
Dead	16 (64%)	8 (73%)

3.1.3 Hepatocellular Cancer

Patients with verified HCC or highly suspected HCC were recruited for this retrospective observational study during 2013-2014. The patients had an additional PCT exam performed in addition to their clinical routine examination. Inclusion criteria were radiological signs of HCC and no previous treatment for HCC of any kind. Patients with lesions larger than 7cm in diameter or more than four lesions were excluded.

A total of 17 patients were included. One patient underwent two PCT scans with a time interval of three months. Those both scans were analyzed separately. The number of identified HCC was 37. Histopathological data verifying the HCC diagnosis was available for eight of the included patients. In the other patients, the European Association for the Study of the Liver (EASL) criteria were used for diagnosis (40). The maximum diameter of each lesion was between 10-55mm.

3.2 Imaging parameters

Study I. MRI 3D T2 weighted FLAIR acquisitions with 1.00 mm slices and no inter-slice gap were used for texture analysis. Echo time, repetition time, inversion time and flip angle (TE/TR/TI/FA) were 389-394/5000/1800/120. T1 weighted images with gadolinium (gadoterate meglumine) were available for the conventional clinical description (e.g.concerning contrast enhancement), but not used for textural analysis. These were acquired as 3D gradient echo sequences with 1.00 mm slices and TE/TR/TI/FA being 2.92/2300/1100/8 or 2.96/2000/1100/8 or 3.16/1900/900/9. Both FLAIR and T1 sequences were done with 1.00 × 1.00 mm pixel spacing in a 256 ×256 matrix. All follow-up MRI exams until reoperation were reviewed according to the criteria from the RANO group (18). Follow-up MRI-exams were performed every 6 months, with shorter intervals of 2–3 months if unclear findings or possible sign of progression, and with intervals of up to 12 months after years of stable disease and no remaining FLAIR-abnormalities.

Study II. The patients underwent multi-slice CT of the thorax using a multi-slice GE Lightspeed VCT (GE Healthcare, WI, USA) or Siemens Somatom Definition Flash (Siemens AG, Erlangen, Germany). All examinations were performed after intravenous contrast injection of Iomeron 400mg I/ml (Bracco, Milan Italy) at 120kV in both arterial and portal phase. The tube current was automatically modulated. The dosage of contrast media was 750mg I/kg or 1000mg I/kg. Slice thickness was 0.625mm. The field of view was adjusted for patient size.

Study III. A single Siemens Biograph 64-slice combined PET-CT scanner (Siemens AG, Erlangen Germany) was used for imaging of CT and FDG-PET-images. At baseline i.e. before neoadjuvant therapy, 27 patients were scanned with the use of intravenous contrast media and 9 without intravenous contrast media. Post-treatment scans were done with the use of intravenous contrast media in 17 patients and 19 without (Table 4). The dosage of contrast media was 1 ml per kilo body weight + 10 ml of Optiray 350 mg I/ml (Guerbet, Roissy, France) and imaging was done in the parenchymal phase and contiguous 1.5 mm thick images were obtained 60 seconds after injection. The field of view was adjusted for patient size during scanning. The dose of 18F-FDG was 400 MBq and uptake time was 60 min.

Table 4 *Presence of intravenous contrast media pre- and post-treatment for included esophageal cancer patients.*

	Adenocarcinoma (*n* = 25)		
Contrast at post-treatment CT exam	Contrast at pre-treatment CT exam		
	+	-	Total post-treatment
+	10 (40%)	3 (12%)	13 (52%)
-	9 (36%)	3 (12%)	12 (48%)
Total pre-treatment	19 (76%)	6 (24%)	

Frequency (%)	**Squamous Cell carcinoma (*n* = 11)**		
Contrast at post-treatment CT exam	Contrast at pre-treatment CT exam		
	+	-	Total post-treatment
+	3 (27%)	1 (9%)	4 (36%)
-	5 (45%)	2 (18%)	7 (64%)
Total pre-treatment	8 (73%)	3 (27%)	

Study IV. Patients were scanned using a single Siemens Definition Flash perfusion CT scanner (Siemens AG, Erlangen Germany). Total number of scan cycles was 26-28. Scan time was between 43-54 seconds with a cycle time of 1.5 seconds between each scan. Tube voltage was 80kV and tube current was 160mAs. Scans were done with the use of intravenous contrast medium at a dose of 50 ml of 400mg Iodine/ml. The flow rate was 6 ml/s and the injection duration was 8.3 s. The scanning direction was alternating craniocaudal and images with 1.5mm slice thickness were used for further analysis.

3.3 Tumor segmentation

Study I. A radiologist experienced with LGG assessment and segmentation performed the semiquantitative data interpretation and segmented the tumors using an open source software called 3D Slicer (http://www.slicer.org/) applying a previously described method (102,103). The radiologist was blinded for clinical result and molecular status while evaluating contrast enhancement (no, patchy, nodular and ring-like), corpus callosum involvement (yes, no), tumor borders, main tumor side, volume in milliliters, and mass effect (no, mild, conspicuous). Tumor borders were radiologically classified as 1) well-defined when the border between tumor and normal appearing brain was sharp; 2) partially absent (vague) when it was still visible, but more diffuse; and 3) absent when tumor growth was very diffuse, and the border was hardly possible to establish (102).

Study II. A second-year resident in radiology and a consultant radiologist with 25 years of experience independently measured the tumor volume in 23 patients with esophageal cancer (middle and distal third part) by manual and semiautomatic segmentation.

The segmentation was performed using a dedicated workstation with GE AW 4.0 (GE Healthcare, WI, USA).

Images were first reformatted to 2.5 mm and displayed as average intensity projections. CT window level settings were at the discretion of the observer. Only transaxial images were available for the observers. For the semiautomated segmentation, the first and last slice containing the primary esophageal tumor, and slices where major morphologic changes occurred, were delineated manually using a mouse-controlled cursor. The rest of the tumor was then first interpolated by the software and the resulting volume of interest was reviewed by the radiologist and manually adjusted by adding or removing included tumor area for each slice where disagreement with the software interpolated selection occurred. The lower and higher threshold of voxels included in the volume of interest was set to 0 and 1000 Hounsfield units respectively in order to exclude air and include all esophageal tumor tissue. The cross-sectional areas of all slices were multiplied by the slice thicknesses and the total volume was calculated by summation of these volumes. The measurement of the tumors was done in both arterial and venous phase for each patient, resulting in two measurements of volume per tumor per observer.

The manual segmentation was done by the same observers at least three months after the measurement using semiautomated segmentation to reduce the effects of recall of the previous semiautomated segmentation. The tumor was manually delineated on transaxial images on every slice containing the primary esophageal tumor and tumor volume was calculated by multiplying cross-sectional areas of all slices by the slice thickness and summation of the resulting volumes.

Study III. The same senior consultant radiologist as in study II segmented the tumor volume of all included patients from 1.5mm image slices. The segmentation was done using a similar semiautomatic segmentation technique as in study II, but instead of the GE software, an open source software called ImageJ 1.50e (Bethesda, Maryland, USA) (104) with the Segmentation Editor plugin 2.0.2 was used (105).

Study IV. The lesions were first marked out on the CT images by a consultant radiologist. The same senior consultant radiologist as in study II and III manually segmented the lesion on the center time point of the perfusion CT series using the slice with the largest area. As in study III, ImageJ 1.50e was used for the segmentation. The resulting region of interest (ROI) was then copied to the other time points. The positioning was adjusted in order to compensate for movement due to breathing when necessary. A junior radiologist then segmented normal hepatic tissue close to the segmented lesion on all time points. Median area of the ROI was 2.7 cm^2 for lesions and 5.8 cm^2 for normal hepatic tissue.

3.4 Textural analysis

Study I. Haralick textural parameters were extracted from the segmented tumor volume in the MRI image material (73). The analysis was limited to Energy, Entropy, Homogeneity, Inertia, and Correlation, as some textural parameters have been shown to be redundant in previous studies (75). Each textural parameter was calculated based on the grey level co-occurrence matrices (GLCM) calculated for all voxels in the segmented tumor volume. Each textural parameter describes a relation of voxels with their local neighborhood, as detailed in Table 5. The signal intensities in the MRI image data was rescaled to 256 grey levels for GLCM calculations. The GLCM was computed using 256 bins and using offsets in all 26 directions. The texture features were computed using an in-house written plug-in for ImageJ 1.50e (104).

Study III and IV. The same textural parameters as in study I were used in this study. The Hounsfield unit data of all voxels in the segmented region or volume were rescaled to 256 grey levels for GLCM calculations. The textural parameters were then calculated based on GLCM obtained using the plug-in developed for ImageJ in study I.

Table 5 *Texture analysis parameters used for processing of image data.*
i and j refers to the bins in the grey level co-occurrence matrices, p(i,j) to the value of the marginal-probability at point (i,j)

Energy	Describes the similarity of voxels in the region. $\sum_{i,j} p(i,j)^2$
Entropy	Describes the disorder in the distribution of gray levels in the region. $-\sum_{i,j} p(i,j) log(p(i,j))$
Correlation	Describes the correlation between voxel pairs in the region $\sum_{i,j} \frac{(i-\mu_x)(j-\mu_y)p(i,j)}{\sigma_x \sigma_y}$
Homogeneity (Inverse Difference Moment)	Describes the homogeneity of the co-occurrence pairs $\sum_{i,j} \frac{1}{1+(i-j)^2} p(i,j)$
Inertia (Contrast)	Describes the variation in signal intensities $\sum_{i,j} (i-j)^2 p(i,j)$

3.5 Statistical analysis

Statistical analysis was done using R 3.2.3, (R Foundation for Statistical Computing, Vienna, Austria) for study I and a more recent version, R 3.4.3 for study II, III and IV (106).

Statistical significance for all studies was defined at a level of $p < 0.05$. Data are presented as median values (interquartile range, IQR) in study I and III and as mean values (95% confidence interval of the mean, CI) in study II. Mean difference was tested using Mann-Whitney U test with tie correction in study I, II, III and IV.

Study II. Intraclass correlation coefficients (ICC) were calculated for intra- and interobserver measurements. Significance of difference in correlation was tested using a Fisher r to z calculation. The level of observer agreement was characterized further using Bland-Altman plots to graphically visualize the level of agreement. Upper and lower limits of agreement were calculated and incorporated into the plots (107). Observer measurement accuracy was also assessed by calculating the average absolute difference from mean for each tumor volume measurement. Comparison of measured tumor volume between arterial phase and portal-venous phase was used to assess intraobserver variability of measurement.

Study III. For analysis of the prognostic value of textural parameters for overall survival, patients were divided into at a cut-off at 1 year into a short (< 1 year) overall survival group and a long (> 1 year) overall survival group.

Median survival and follow-up time were calculated using the Kaplan-Meier and reverse Kaplan-Meier method (108).

Study IV. Linear regression was used to determine drift of textural parameters over all time points.

3.6 Ethical considerations

All participants in the included studies of this thesis provided written informed consent.

Approval for study I was granted by the regional ethical committee of Central Norway, reference number 2016/1377.

Ethical approval for study II and III was granted by the regional ethical review board in Stockholm, approval number: DNR 2008/403-32.

Ethical approval for study IV was granted by the regional ethical review board in Stockholm. Approval numbers were DNR 2013/1072-32 and DNR 2013/405-31.

4 RESULTS

4.1 Study I - Textural analysis of low-grade glioma

Imaging characteristics and textural parameters from MRI data are presented in Table 6. The textural parameter Homogeneity was significantly different depending on *IDH* mutation status, as shown in Figure 4. Homogeneity for individual patients in relation to molecular profile (i.e. *IDH*wt, *IDH*mut, *IDH*mut and 1p-19q codeletion) is presented in Figure 5.

No significant correlations to *IDH* mutation status were observed for the other textural parameters. Good classification results for both Homogeneity and tumor volume were observed in receiver operating characteristic (ROC) curves for *IDH* mutation status. When combining Homogeneity and tumor volume in correlation to *IDH* status by logistic regression using a generalized linear model, good classification results was observed (Figure 6). The area under the curve (AUC) for predicting *IDH* mutation was 0.905 for Homogeneity, 0.840 for tumor volume and 0.940 for the combined parameters of tumor volume and Homogeneity.

Table 6 *Imaging characteristics of low-grade glioma patients. IQR = Interquartile range.*

Energy, median (IQR)	0.0009 (0.0004- 0.0010)
Entropy, median (IQR)	7.9 (7.2 - 8.0)
Homogeneity, median (IQR)	0.12 (0.09 - 0.13)
Inertia, median (IQR)	329 (213 - 514)
Correlation, median (IQR)	0.0010 (0.0009 - 0.0020)
Contrast enhancement	
No	19 (76%)
Patchy	5 (20%)
Nodular	1 (4%)
Ring-like	0 (0%)
Corpus callosum involvement	2 (8%)
Tumor border	
Absent	6 (24%)
Vague	9 (36%)
Conspicuous	10 (40%)
Mass effect	
No	17 (68%)
Mild	7 (28%)
Conspicuous	1 (4%)
Main tumor side	
Left	13 (52%)
Right	12 (48%)
Main lobe involved	
Frontal	12 (48%)
Temporal	6 (24%)
Insula	7 (28%)
Eloquence*	10 (40%)
Tumor volume, median in ml (IQR)	27 (7-37)

*As defined by Chang et al (109)

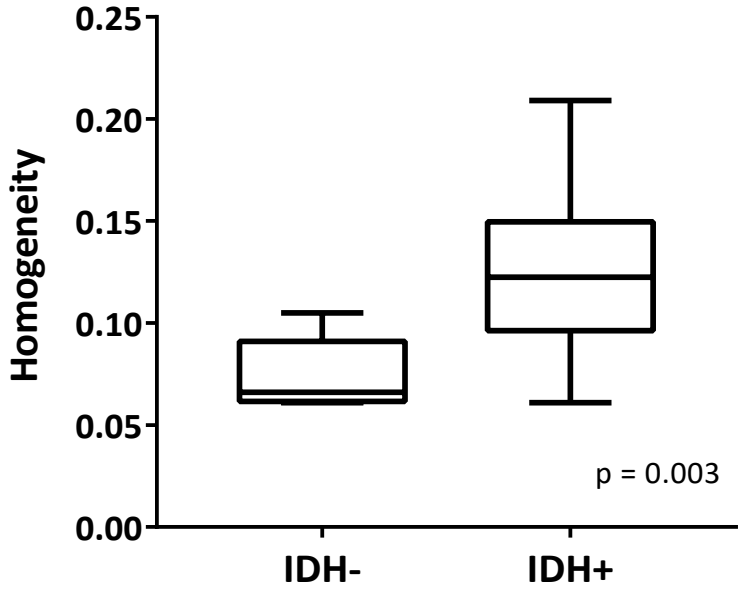

Figure 4 *Difference in Homogeneity between patients with (median 0.12,range IQR 0.10-0.15) and without (median 0.07, range IQR 0.06-0.09) IDH mutation (p=0.005). Whiskers show minimum and maximum value. There was a significant difference in Homogeneity when comparing groups.*

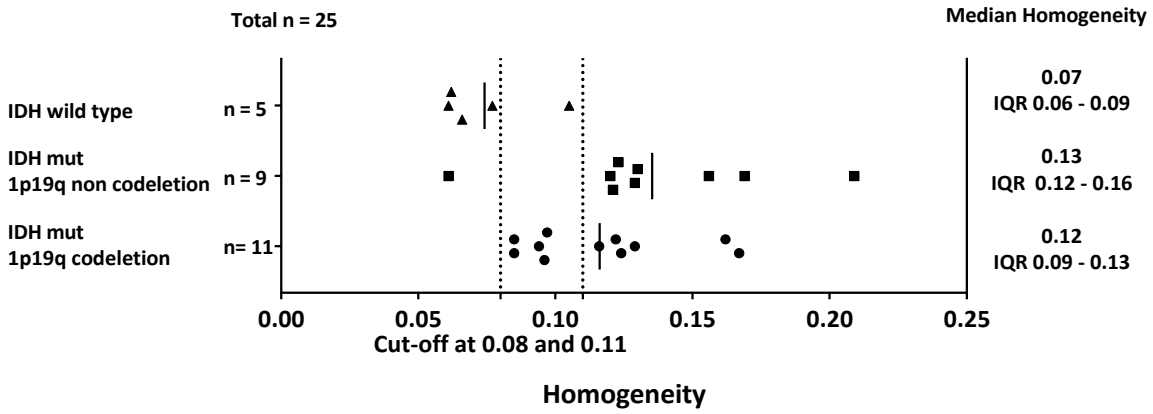

Figure 5 *Presentation of individual patients MRI FLAIR Homogeneity in relation to molecular status, example cut-offs are given at 0.08 and 0.11*

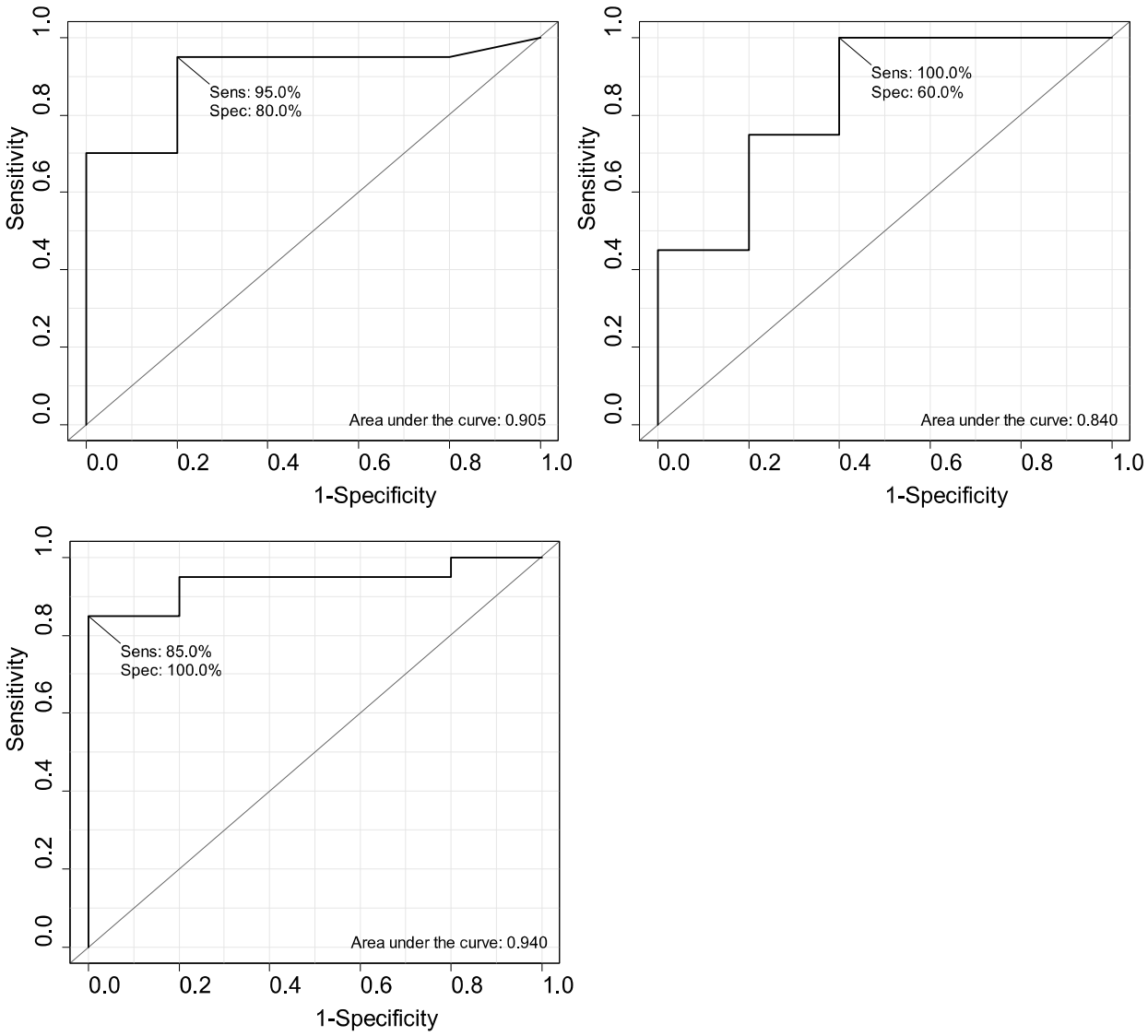

Figure 6 *ROC curves for IDH mutation status correlated to Homogeneity (upper left), tumor volume (upper right) and a linear model combining Homogeneity and tumor volume (lower left).*

4.2 Study II – Comparison of semiautomated and manual segmentation

All tumors were detected for all included patients by both observers. Mean tumor volume was 46 ml (range 5-137 ml) using manual segmentation and 42 ml (range 3-111 ml) using semiautomatic segmentation when arterial and portal-venous measurements was merged, (p = 0.30). No significant differences in volume were observed between adenocarcinoma and squamous cell carcinoma (Table 7).

Table 7 *Measured primary esophageal tumor volume for all included patients by radiology resident and radiology consultant using manual and semiautomatic segmentation. All volumes measured in milliliters (ml).*

	Manual				Semiautomatic			
	Resident		Consultant		Resident		Consultant	
	Arterial	Venous	Arterial	Venous	Arterial	Venous	Arterial	Venous
1	15	14	5	5	33	31	3	3
2	42	44	13	8	36	31	24	28
3	36	44	5	6	23	26	25	25
4	44	50	16	15	28	21	26	25
5	57	52	30	33	48	59	29	35
6	46	54	43	31	39	33	33	36
7	105	99	62	63	70	83	68	74
8	135	125	81	70	95	101	69	68
9	51	66	21	23	34	42	19	26
10	65	56	23	35	47	40	41	40
11	137	132	73	78	111	110	92	104
12	73	81	58	59	59	62	59	54
13	66	69	45	48	50	50	40	38
14	27	35	17	17	19	22	17	16
15	49	64	36	36	47	55	28	31
16	32	30	24	24	18	24	20	25
17	56	46	35	32	44	34	38	38
18	59	44	36	32	77	77	80	75
19	51	57	42	44	39	47	37	41
20	48	48	11	12	28	36	20	19
21	25	42	11	12	13	19	10	14
22	41	38	24	29	16	15	20	28
23	69	75	51	47	55	62	52	53
Mean (CI 95%)	58 (44-71)	59 (47-72)	33 (24-42)	33 (24-42)	45 (34-55)	47 (36-58)	37 (27-47)	39 (29-49)

4.2.1 Intraobserver variability of tumor assessment at CT

No statistically significant difference of mean tumor volume was observed for both manual and semiautomatic methods for both observers between arterial and portal-venous volume measurements. An excellent intraobserver agreement with ICC of 0.97 for both manual and semiautomatic segmentation was observed when comparing arterial tumor volume with portal-venous volume. Low variability was observed in Bland-Altman plots (Figure 7A, C) in comparison to interobserver variability.

4.2.2 Interobserver variability of tumor assessment at CT

Semiautomatic segmentation showed a significantly higher interobserver ICC in comparison to manual segmentation (0.86 versus 0.56, $p < 0.01$). Slightly narrower limits for semiautomatic segmentation in comparison to manual segmentation, (40.1 ml versus 56.8 ml) was observed in Bland-Altman plots (Figure 7B, D). ICC was significantly higher for semiautomatic segmentation compared to manual segmentation for measurements of adenocarcinoma (0.86 versus 0.54, $p < 0.01$) but not for squamous cell carcinoma (0.88 versus 0.63, $p = 0.052$). No significant differences in ICC between adenocarcinoma and squamous cell carcinoma were detected when sub-analyzing the manual segmentation or semiautomatic segmentation group.

The average absolute percentage difference from mean tumor volume was significantly lower when using semiautomatic segmentation (14 %, CI:9%-19%) compared to manual segmentation (32 %, CI: 26%-37%, $p < 0.001$, Figure 8). The difference of percentage was significantly lower for squamous cell carcinoma compared to adenocarcinoma (23%, 36%, $p < 0.05$) when using manual segmentation. This difference was not observed for semiautomatic segmentation.

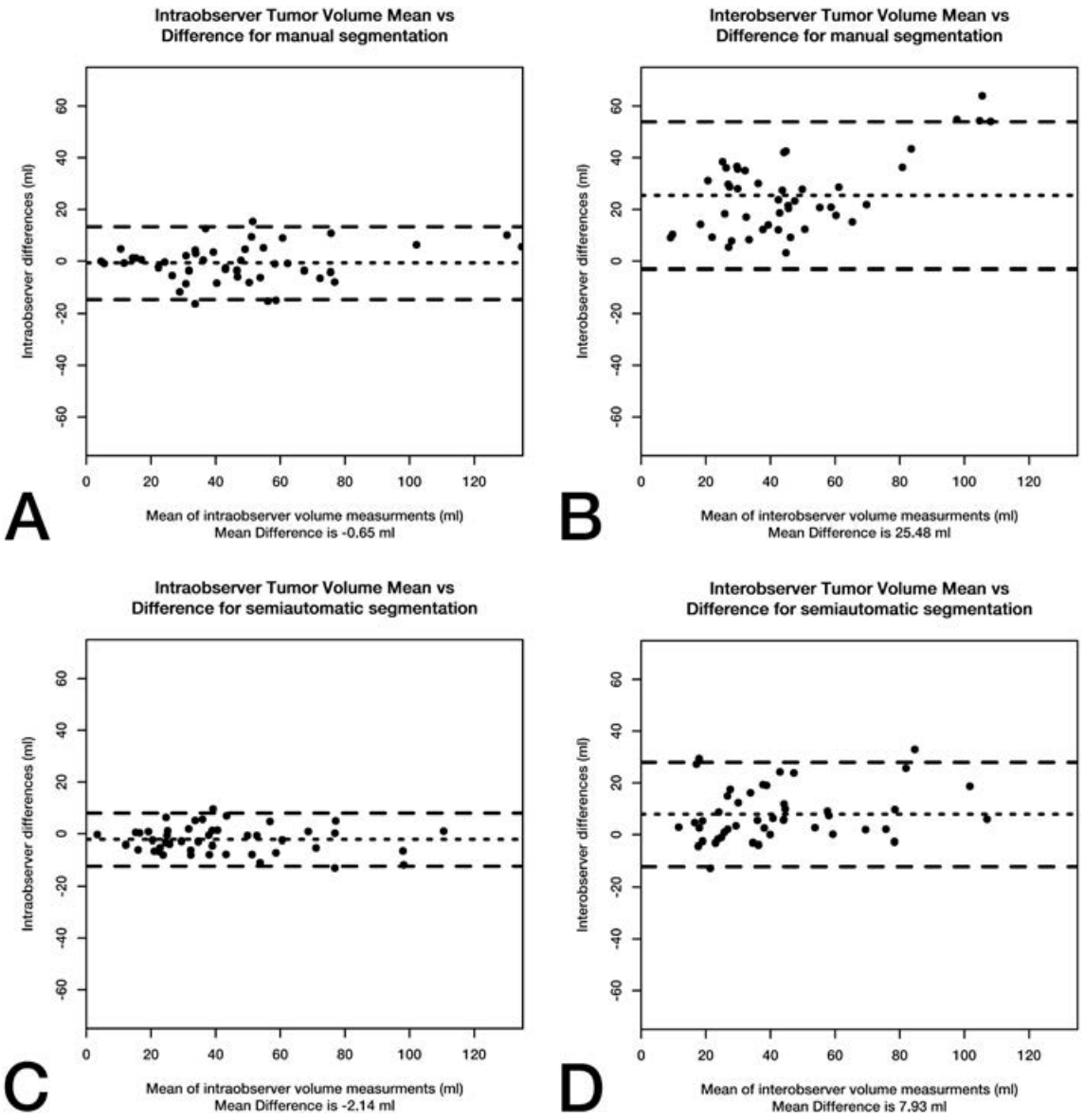

Figure 7A-D *Bland-Altman plots for intraobserver and interobserver differences during tumor volume measurement using manual and semiautomatic segmentation. The difference of tumor volume is plotted against the mean. The dashed lines are calculated as ±1.96SD and show upper and lower limits of agreement. The dotted line shows the mean difference.*

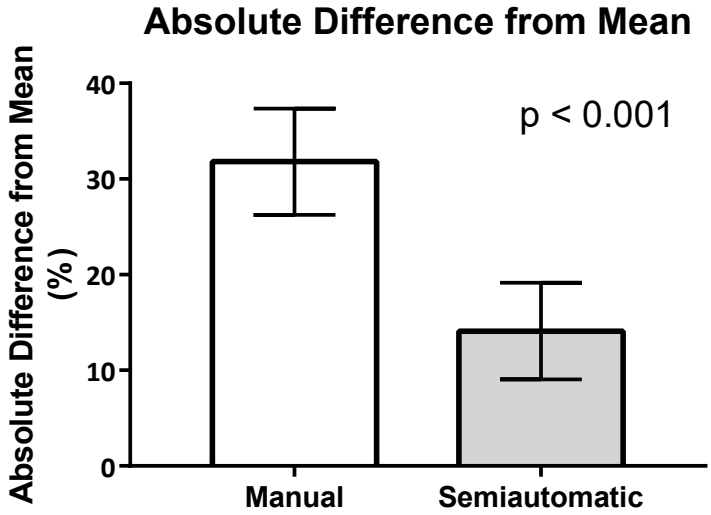

Figure 8 *Mean absolute differences from the mean measured volume of esophageal tumor by use of semiautomatic segmentation and manual segmentation, respectively.*

4.3 Study III – Textural analysis of esophageal cancer

4.3.1 Differences of segmentation between CT and PET-aided CT images

The mean difference in tumor volume between the PET-aided CT image segmentation and the segmentation using only CT image data was -17 ml, (-27 ml – -7 ml, CI 95%) corresponding to 28%, (-41% – -16%, CI 95 %) for adenocarcinoma and -9 ml, (-14 ml – -5 ml, CI 95%) corresponding to -26%, (-39% – -13%, CI 95%) for squamous cell carcinoma. These small differences between adenocarcinomas and squamous cell carcinomas did not reach statistical significance.

There was no significant difference in the textural parameters between volumes segmented using PET-aided CT image segmentation and segmentation using CT images alone. The exclusion of the segmented metabolically inactive tumor volume using PET did not affect these outcomes.

4.3.2 Textural parameters and histological typing

Significant differences between adenocarcinoma and squamous cell carcinoma were detected in Homogeneity, Energy, Inertia, and Correlation among patients receiving intravenous contrast during examination as shown in Figure 9. There was also a significant difference in Homogeneity, Energy, Entropy and Inertia for AC depending on whether patients had received contrast media at the imaging. This was not observed for SCC. No significant differences in tumor volume were detected between any of the groups (i.e. AC and SCC, without and with contrast media).

There was a significant difference in all textural parameters between post neoadjuvant pathological tumor (ypT) status ypT0-ypT2 and ypT3-ypT4 for esophageal AC patients (Figure 10), but not for esophageal SCC patients (Table 8). No significant difference in volume was detected between ypT0-ypT2 and ypT3-ypT4 AC and SCC.

No significant difference of correlations between textural parameters and histological type was found between PET-aided CT image segmentation and CT only segmentation.

Table 8 *Means of volume and textural parameters at contrast-enhanced CT compared among neoadjuvant pathological tumor status (ypT) for esophageal adenocarcinoma and squamous cell carcinoma for morphologic (CT)/metabolic (PET) delineation of tumor*

	Adenocarcinoma (n=19)			**Squamous cell carcinoma (n=8)**		
Parameter	**ypT0-2**	**ypT3-4**	**p**	**ypT0-2**	**ypT3-4**	**p**
Volume (ml)	73/62	63/43	0.5/0.43	85/75	21/15	0.25/0.79
Homogeneity	0.057/0.057	0.070/0.069	**0.002/ 0.010**	0.079/0.78	0.085/0.078	0.79/0.79
Energy	0.000285/ 0.000288	0.000385/ 0.000392	**0.010/ 0.010**	0.00050/ 0.00051	0.00045/ 0.00051	0.79/>0.99
Entropy	8.50/8.49	8.25/8.24	**0.010/ 0.010**	8.07/8.05	8.13/8.05	0.57/>0.99
Inertia	494/497	346/352	**0.001/ 0.004**	315/319	251/244	0.79/0.79
Correlation	0.00090/ 0.00087	0.00146/ 0.00087	**0.002/ 0.005**	0.0019/ 0.0019	0.0020/ 0.0019	>0.99/0.79

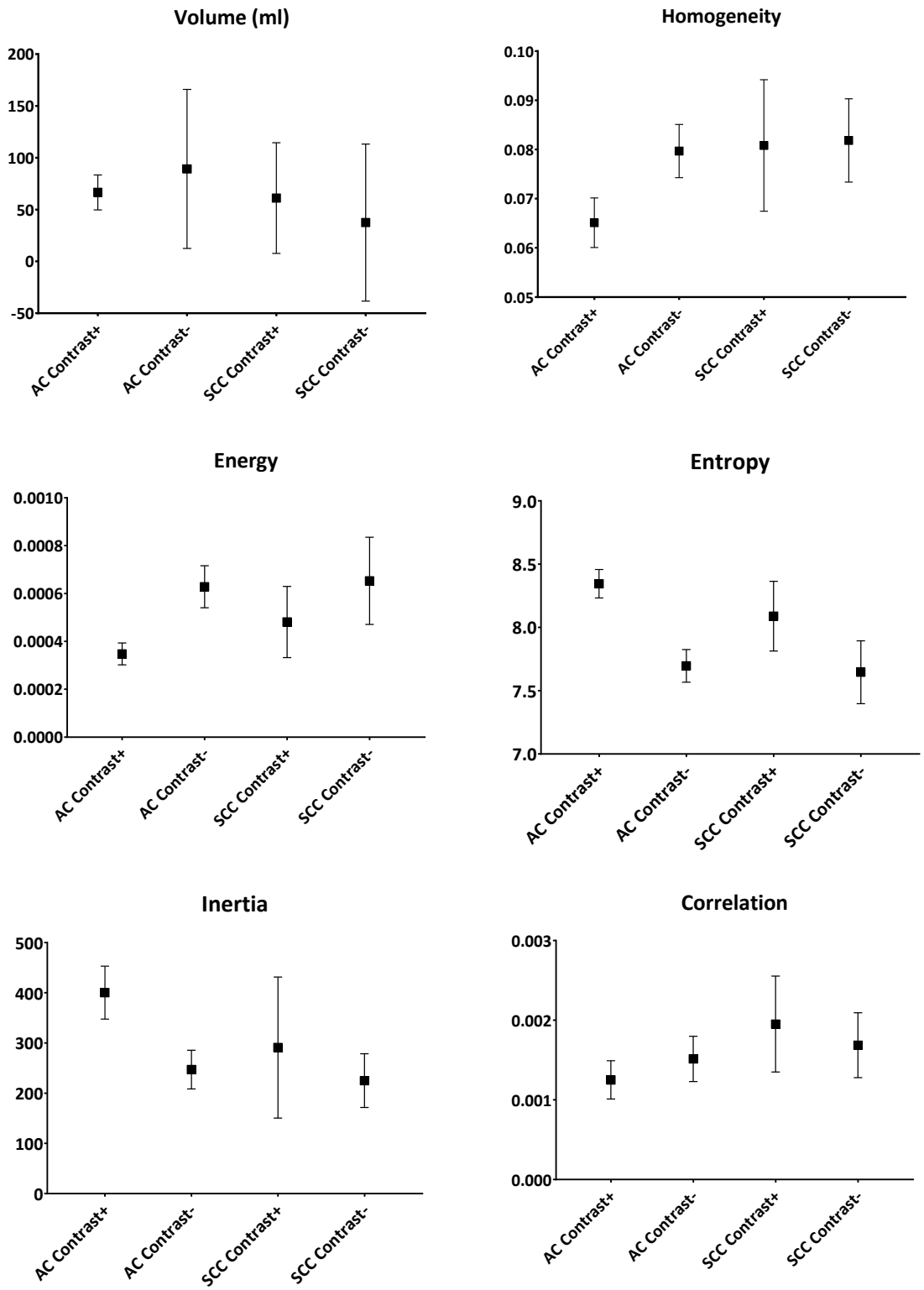

Figure 9 *Comparison of textural parameters at morphologic (CT) delineation of tumor between esophageal adenocarcinoma (AC) and squamous cell carcinoma (SCC), pre-neoadjuvant therapy between patients with and without intravenous contrast during examination. Figures show means with 95% confidence interval error bars.*

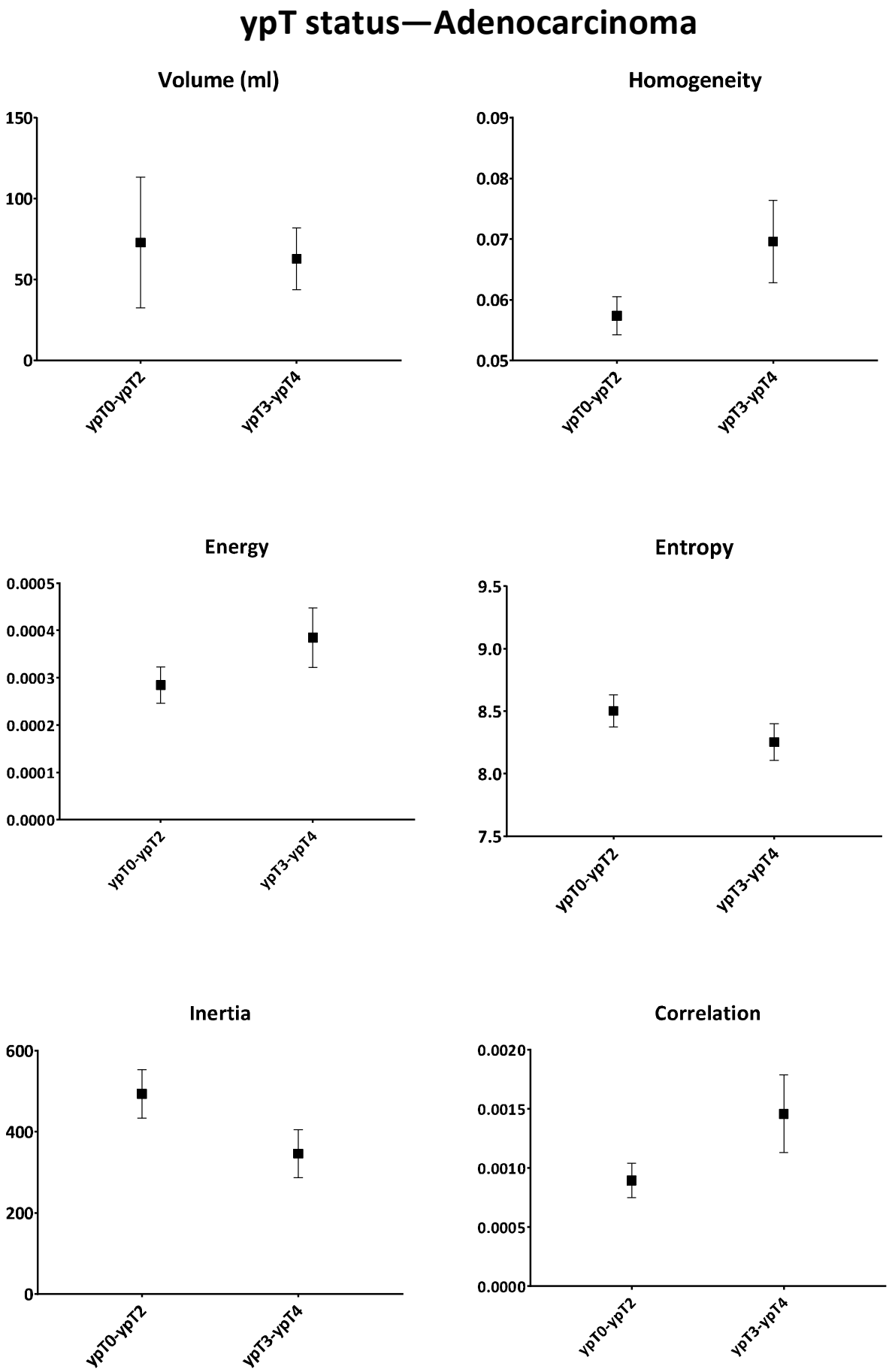

Figure 10 *Neoadjuvant pathological T (ypT) status of surgically removed esophageal adenocarcinoma compared with textural parameters at morphologic delineation (CT) of tumor and segmented volume. Figures show means with 95% confidence interval error bars.*

4.3.3 Textural parameters and overall survival

The median overall survival of all included patients was 19.3 months (adenocarcinoma 18.6 months; squamous cell carcinoma 20.0 months). Median follow-up time was 96.4 months (adenocarcinoma 90.5 months; squamous cell carcinoma 102.1 months). A significant difference between short and long survival was observed for tumor volume of adenocarcinoma segmented using PET-aided CT image segmentation. No other significant impact of segmented volumes or any of the textural parameters of contrast-enhanced CT was found (Table 9).

Further sub-analysis of 10 adenocarcinoma patients with pre- and post-treatment exams with intravenous contrast administration did not change the outcome (data not shown).

No effect on the registered variables was observed regardless of the type of neoadjuvant regimen or tumor type.

Table 9 *Means of textural parameters and volume at contrast-enhanced CT compared between short (<365 days) and long (>365 days) overall survival (OS) for esophageal adenocarcinoma and squamous cell carcinoma using morphologic (CT)/metabolic (PET) delineation of tumor.*

	Adenocarcinoma OS (n=19)			**Squamous cell carcinoma OS (n=8)**		
Parameter	**<365 Days**	**>365 Days**	**p**	**<365 Days**	**>365 Days**	**p**
Volume (ml)	44/59	75/24	0.06/**0.03**	20/14	75/65	0.29/0.86
Homogeneity	0.069/0.068	0.064/0.064	0.07/0.11	0.09/0.08	0.077/0.078	0.29/0.29
Energy	0.000358/ 0.0003571	0.000344/ 0.000348	0.39/0.30	0.00048/ 0.00050	0.00048/ 0.00049	0.86/0.43
Entropy	8.30/8.27	8.36/8.36	0.39/0.39	8.04/8.01	8.11/8.09	>0.99/0.43
Inertia	344/350	421/425	0.07/0.11	209/211	318/317	0.29/0.29
Correlation	0.00136/ 0.00132	0.00121/ 0.00119	0.16/0.19	0.0022/ 0.0023	0.0019/ 0.0018	0.43/0.29

4.4 Study IV – Variation in textural analysis parameters during contrast injection of HCC

Injection of contrast medium increased all HCC texture parameters and the parameters Energy and Correlation in non-tumorous hepatic tissue (Table 10). However, the observed slope coefficients (i.e. the respective increase over time) were several magnitudes below the median values of each textural parameter.

After contrast medium injection, the variability in texture parameters in tumors over time was smaller than the variation between different tumors (Table 11), but it was not significant for Inertia. This difference was not observed in normal hepatic tissue, where all parameters showed a higher variability over time in comparison to the variation between different individuals. When comparing the variability in texture parameters after contrast medium injection the parameter Entropy varied significantly less in lesions than in tissue (SD=0.089 versus SD=0.156, $p < 0.05$), while no significant differences were observed in the other parameters. The average of each texture parameter varied more in Energy and Entropy (SD=0.000413 and SD=0.326 respectively) for lesions than hepatic tissue (SD=0.000108 and SD=0.109 respectively), $p < 0.001$ and $p < 0.05$ respectively.

Normalized mean textural parameters for all HCC lesions and normal hepatic tissue ROIs are shown in Figure 11 and Figure 12. A value of one (1) represents equal value as the measured value at the first scan.

Table 10 *Median slope coefficient for linear regression over all time points for each textural parameter for all lesions. The lower quartile (LQ) and upper quartile (UQ) are presented. The median of each textural parameter over all time points is presented in the fourth column. The same data for normal hepatic tissue is also presented.*

Slope, lesions	LQ	Median	UQ	Parameter median
Homogeneity	-0.00022	-0.00009	0.00005	0.076
Energy	-0.0000034	-0.0000014	-0.0000001	0.0011
Entropy	0.00014	0.00065	0.00216	7.05
Inertia	-0.3	0.8	1.7	304
Correlation	-0.0000161	-0.0000046	-0.0000004	0.0015
Slope, tissue	**LQ**	**Median**	**UQ**	**Parameter median**
Homogeneity	-0.00023	-0.00004	0.00000	0.092
Energy	-0.0000034	-0.0000008	-0.0000001	0.00082
Entropy	-0.00005	0.00085	0.00310	7.30
Inertia	-0.3	0.3	1.1	198
Correlation	-0.0000152	-0.0000040	-0.0000001	0.0024

Table 11 *Mean standard deviation for each textural parameters over all time points for each lesion (Intra-lesion) and between all lesions for each time point (Inter-lesion). Data for normal hepatic tissue is also presented.*

Standard Deviation	Intra-lesion	Inter-lesion	p
Homogeneity	0.010	0.014	**0.009**
Energy	0.000187	0.000413	**0.0001**
Entropy	0.089	0.326	**0.00003**
Inertia	91	112	0.25
Correlation	0.00046	0.00060	**0.039**

	Intra-tissue	Inter- tissue	p
Homogeneity	0.012	0.009	0.10
Energy	0.000146	0.000108	0.11
Entropy	0.156	0.109	0.09
Inertia	90	73	0.47
Correlation	0.00063	0.00050	0.29

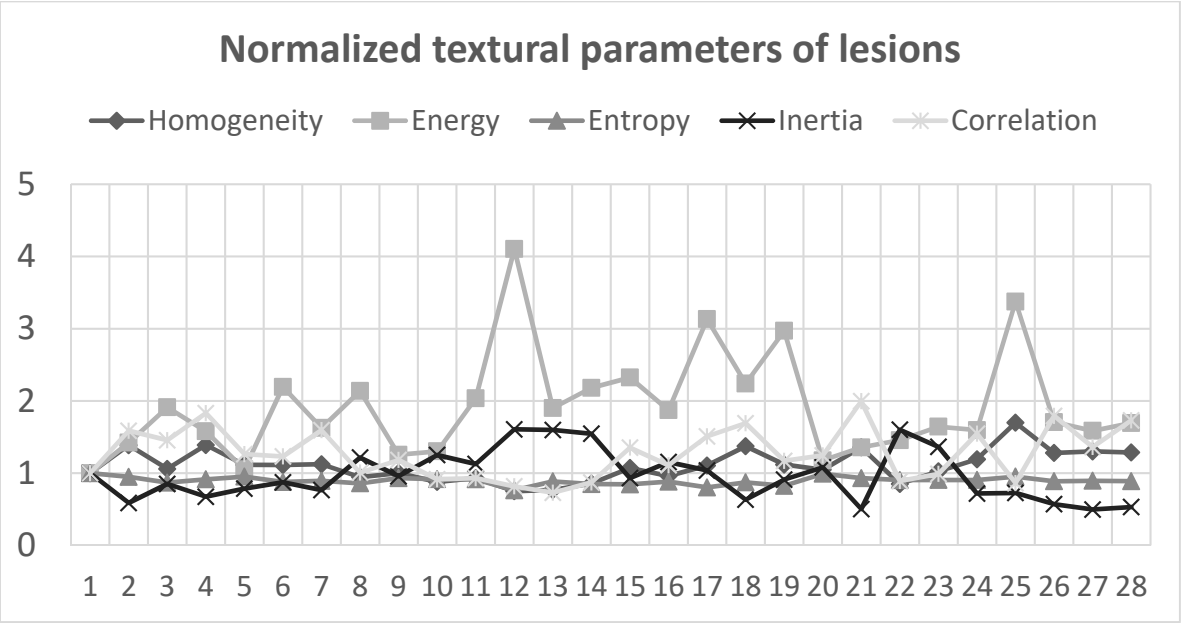

Figure 11 *Normalized mean textural parameters of all lesions over time. X-axis indicates time point, Y-axis the normalized value in comparison to the measured value at the first scan.*

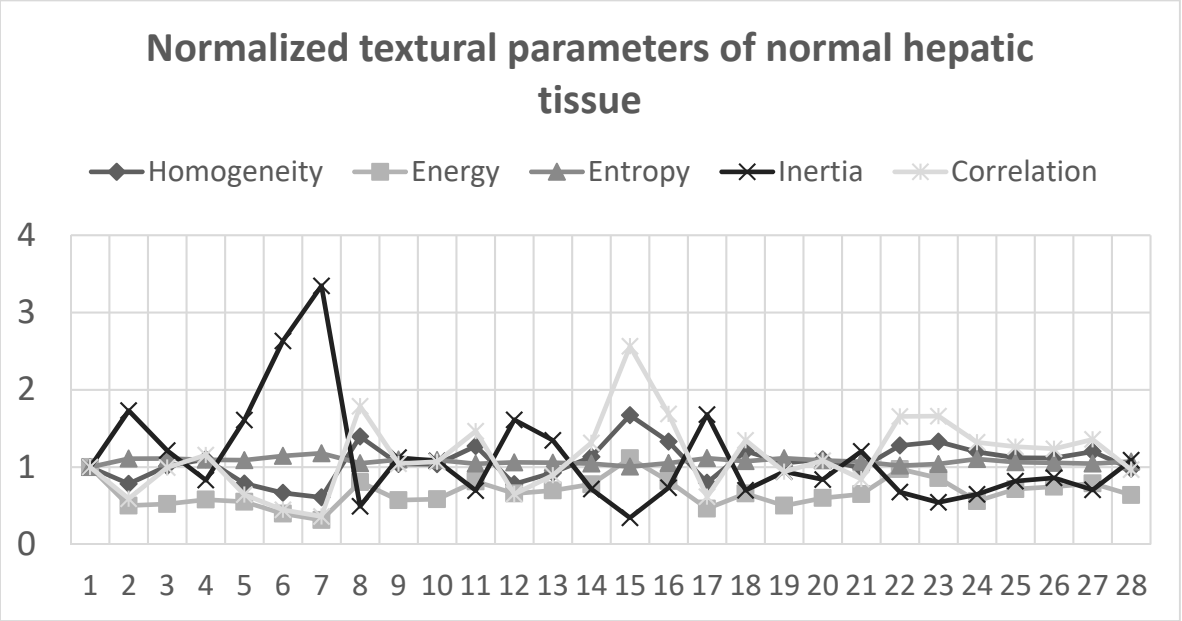

Figure 12 *Normalized mean textural parameters of all normal hepatic tissue ROIs over time. X-axis indicates time point, Y-axis the normalized value in comparison to the measured value at the first scan.*

4.4.1 Comparison of textural parameters between normal tissue and lesions

Significant differences between the mean of each of the textural parameters Energy, Entropy, Inertia and Correlation for normal hepatic tissue and lesions were observed (Table 12). However, only the textural parameter Energy differed more than the 95% confidence interval of the average textural parameter value for normal hepatic tissue (i.e. 1.96 times the standard deviation).

Table 12 *Mean textural parameters for normal hepatic tissue in comparison to lesions. Whether the observed difference is beyond 1.96 times the observed intra-tissue standard deviation (SD) for significantly different parameters is also presented.*

	Tissue	Lesion	p	Beyond 1.96SD
Homogeneity	0.089	0.080	0.12	N/A
Energy	0.0009	0.0013	**0.02**	**Yes**
Entropy	7.32	7.03	**0.02**	No
Inertia	263	322	**0.04**	No
Correlation	0.0024	0.0015	**0.002**	No

5 DISCUSSION

5.1 Textural analysis

Through study I and III, it could be shown that textural analysis of MR and CT images yield additional information about tumor histology. In study I, a correlation between Homogeneity and *IDH* mutation status in LGG was found. In study III, differences in textural parameters could be detected between esophageal adenocarcinoma and squamous cell carcinoma. Furthermore, there were differences detected in textural parameters between ypT0-2 and ypT3-4 stage adenocarcinomas.

5.1.1 Considerations when using textural analysis

Because there are several steps between the acquisition of image data and the calculation of textural parameters, there are several issues that have to be considered for each step in order to allow comparison between different studies.

The usual sources of variability through differing imaging protocols, scanner types, slice thicknesses etc have been shown to affect the resulting textural parameters. Validation studies have shown that textural parameters vary about one standard deviation (SD) when using differing scanners and 19% repeatability when different slice thickness and reconstruction algorithms are used (98,99). In study I, III and IV, all included patients were imaged using the same scanner using the same imaging parameter in order to reduce those effects. The importance of keeping the same imaging conditions was seen in study III, where significant differences were observed in textural parameters of segmented tumors between native and contrast-enhanced examinations.

As there are several different parameters that can potentially be analyzed, with some of them sharing the same or similar names, it is of importance that the specific formula used to calculate the parameter is described, so that there is no confusion between parameters using the same name but differing in calculation method. For study I, at least two different formulae for calculating Homogeneity was found and the one described by Haralick was used as it seemed to be the more commonly used. The parameters described by Haralick were used in the following studies III and IV as it had been shown in study I that those parameters had the potential to be useful.

The implementation of the formula in the software used for the respective calculation varies between currently available software. The GLCM textural analysis methods used in this thesis assess the relation between two voxels, thus an important aspect is whether the software analyzes a singular slice in four possible directions on a 2D slice, or if a 3D analysis of the 13 directions in an entire volume is supported. There was no available software for 3D textural analysis at the time the studies in this thesis were planned. Thus a plug-in for ImageJ was implemented to enable calculation of the textural parameters from segmented tumor volumes. More software options are available today, but many are still limited to analyzing single 2D slices (89). As the number of analyzed voxels is a confounding factor for

calculation of textural parameters, there is a suggestion that at least 200 voxels should be included (110). This limits the potential applications for software only capable of analyzing single slices, as these would include only a fraction of the voxels available. This is especially important when analyzing tumors with perpendicular growth to the imaging plane, such as esophageal cancer tumors (Figure 13).

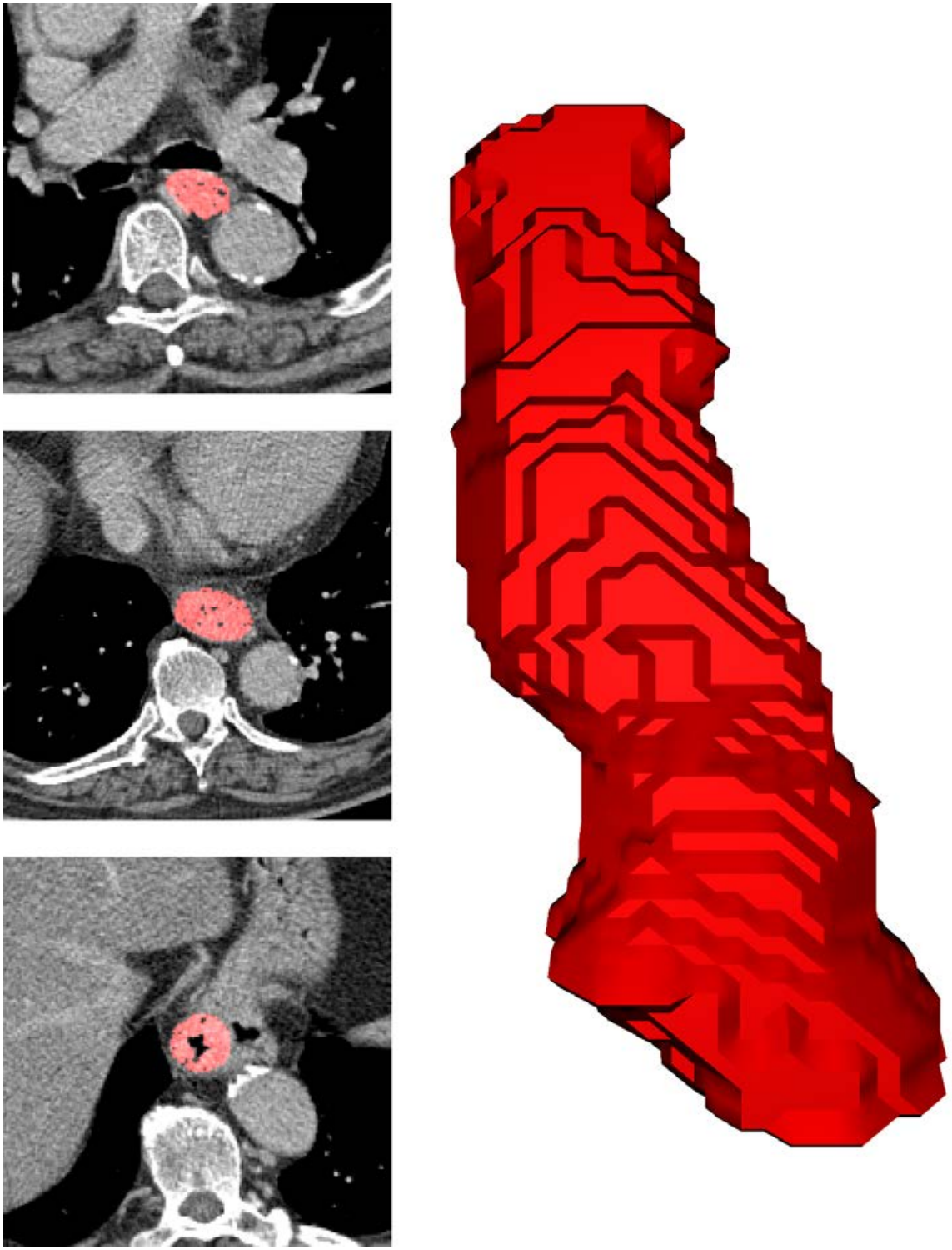

Figure 13 *3D visualization of segmented adenocarcinoma esophageal tumor neoadjuvant pathological stage ypT3N1 from a 64-year old male, illustrating perpendicular growth relative to the transaxial plane. Left images illustrate segmentation of upper, middle and lower areas of the tumor.*

The segmentation of the tumor volume also affects the calculated textural parameters. To reduce the variation in parameters due to differences in segmentation, various automated and semiautomated segmentation methods have been evaluated (59,67,68). However, manual segmentation is still commonly used to segment the volumes used for further analysis. In study II, a reduction of mean differences of tumor volume between two radiologists was observed, showing an improvement in interobserver agreement when using a semiautomated segmentation instead of a manual segmentation method. On the other hand, no further information of interest was found in study IV when using PET information to improve segmentation on CT images of esophageal cancer.

In conclusion, all these factors add to the complexity of planning studies exploring textural analysis and have to be considered when comparing different studies with each other. Even though using similar concepts, differences in inclusion of image data, choice of parameters, specific implementation and segmentations differences could render different results for similar studies.

5.2 Study I - Textural analysis of low-grade glioma

This study showed that the textural parameter Homogeneity can be used to predict mutation status of the *IDH* gene for low-grade glioma and serves as a proof of concept for the plugin developed for ImageJ and later used for calculating textural parameters in study III and IV.

The results suggest that a lower Homogeneity is associated with *IDH*wt mutation status, which has a more aggressive course in comparison to *IDH*mut. This is consistent with other studies of both LGG and also findings of higher heterogeneity of high-grade gliomas compared to LGG (86). Since *IDH*wt LGG prognosis is similar to glioblastoma, early stratification is clinically useful. Tumor growth rate is the currently used prognostic marker (111), but to determine this requires several scans and add delay until treatment, which potentially can be avoided through stratification using textural analysis. Another advantage of textural analysis in comparison to other potential radiogenomic methods such as MR spectroscopy or diffusion-weighted imaging is that no additional scanning is required to gain additional information. This also enables retrospective analysis of already acquired image data and reduces the need for changes of clinical protocol or equipment. The emergence of synthetic MRI (112) might also reduce the variability due to different scanner and parameter choices, improving comparability of textural parameters.

Some limitations of this study were the small number of included patients and lack of comparison with other potential radiogenomic methods such as MR spectroscopy or diffusion-weighted imaging. However, this reflects the current clinical conditions and the limitations of a retrospective study design, as LGG is relatively rare and only cases with imaging indicated by current guidelines are available.

5.3 Study II – Comparison of semiautomated and manual segmentation

It was shown that an improvement can be achieved by using semiautomated segmentation instead of manual segmentation and that semiautomated segmentation can reduce the effects of discrepancies in skill between radiologists for volumetry measurements.

However, there were still differences between the observers, which could be attributed to the properties when imaging esophageal tumors. Due to low contrast between tumor and normal tissue, it was challenging to delineate the cranial and caudal extent of the tumors, particularly for tumors situated at or close to the gastro-esophageal junction. These effects can probably be reduced by using more complex imaging protocols utilizing antispasmodic agents and positive or negative oral contrast media just prior to the CT examination (113,114). However, these protocols are not commonly used in clinical routine practice and could be difficult to implement. The included CT scans in this study did not include multiplanar reformations, which could have aided in the delineation of tumor borders.

The use of other imaging modalities such as FDG-PET-CT could also help to delineate tumor boundaries. The highlighting provided by FDG uptake pinpoints the position of active tumor tissue and helps distinguish it from normal tissue. However, inflammation also causes increased FDG uptake. As inflammation often appears around esophageal tumors (115–117), this could lead to an overestimation of tumor volume. As proper volume segmentation is of importance for the calculation of textural parameters, the effects on esophageal tumor volume measurements by using FDG-PET information in addition to CT images was further examined in study III.

Limitations of this study were the limited number of patients and readers, and the use of two different CT scanners for the examinations. However, the use of different scanners should have no effect on interobserver variance of volume measurement, as both observers are measuring the same images.

5.4 Study III – Textural analysis of esophageal cancer

The primary finding of this study was a correlation between the textural parameters Energy, Entropy, Correlation, Homogeneity or Inertia and ypT-status for esophageal adenocarcinoma, which was not present for squamous cell carcinoma. There were also significant differences in the parameters Homogeneity, Energy and Entropy between esophageal adenocarcinoma and squamous cell carcinoma. However, no association between textural parameters and overall survival was detected.

The growth of esophageal tumors along the axis of the organ and perpendicular to the imaging plane results in a small area for each slice. By analyzing the textural analysis in 3D using a volumetric approach, a sufficient number of voxels could be included to mitigate variation due to insufficient included voxels. The observed lack of correlation between the textural parameters and overall survival is in contrast to other similar studies, where a correlation between textural parameters and overall survival was found (55–57). However, those studies used a different software, which calculated the parameters on a singular transaxial slice and performed an additional Gaussian-filtering step before the calculation. Also, the NeoRes study (101), from which the patients in this study were included, was designed to differentiate tumor response after two different treatment strategies and it was underpowered for survival analysis. The proportion of the patients from that study included here (approximately 20%) would consequently make this study underpowered for such a survival analysis.

In contrast to earlier studies, esophageal adenocarcinoma and squamous cell carcinoma were analyzed separately, as they are considered to be different diseases (27). This view was further supported by the observed significant differences in textural parameters between adenocarcinoma and squamous cell carcinoma. Also, the differences in textural parameters dependent on ypT-status observed for adenocarcinoma but not for squamous cell carcinoma support that they should be analyzed separately when calculating textural parameters.

The studies that the current 8th edition AJCC/UICC Staging Manuals for esophageal cancer is based upon have shown a negative correlation between higher ypT-stage and overall survival (118). The observed correlation of ypT-stage and textural parameters suggests that textural analysis could potentially be a useful method for non-invasive staging of esophageal adenocarcinoma prior to neoadjuvant therapy and surgical resection.

As mentioned earlier, the use of different scanner settings and contrast medium protocols all affect the textural analysis. Therefore, a strength of this study was that all scans were performed using the same scanner with the same imaging settings. However, the usage of contrast medium differed both between patients and between examinations for the same patients, which reduced the number of examinations that could be used for analysis.

Limitations of this study include the different neoadjuvant treatment used for the included patients and the small number of patients for each tumor type, which precluded analysis of textural parameters between the different choices of neoadjuvant treatment. Another limitation was the use of a single observer for tumor segmentation, which could lead to segmentation errors. This risk was reduced by using a semiautomatic segmentation tool and a highly experienced radiologist. Good intraobserver consistency has previously been shown when using manual segmentation (31), and use of semiautomatic segmentation leads, as shown in study II and another study, to further improvement (67).

5.4.1 Additional value of PET for CT Textural analysis of esophageal cancer

The addition of PET image data to aid CT image segmentation did unexpectedly not result in any additional prognostic value for esophageal cancer despite theoretically allowing for a more accurate segmentation by highlighting areas with tumor activity. This could not be explained by a potential mismatch between PET and CT images due to the simultaneous acquisition of those.

The use of PET as an aid for segmentation of CT images, instead of directly analyzing the PET images, reduces the effects of PET-specific limitations i.e. noise artifacts and larger voxel size (119). Those could otherwise potentially cause confounding effects due to lower number available voxels for analysis. However, the variation in metabolic activity within the segmented volume was not analyzed in this study.

The volume of the tumors was on average 26-29% smaller when segmented using PET-aided CT segmentation compared to when using CT segmentation only (Figure 14). This suggests that necrotic, inactive tissue could be excluded from the segmented volumes by using PET data. However, there was no significant difference in the textural parameters between the included and excluded volumes. Consequently, the previously observed differences between adenocarcinoma and squamous cell carcinoma in textural parameters when using only CT information remained and the observed correlation between ypT-status and textural parameters was unaffected.

As the CT image segmentation without and with PET image aid was performed during the same session for each patient, a limitation for these comparisons was the apparent risk of a recall bias when performing the PET aided segmentation.

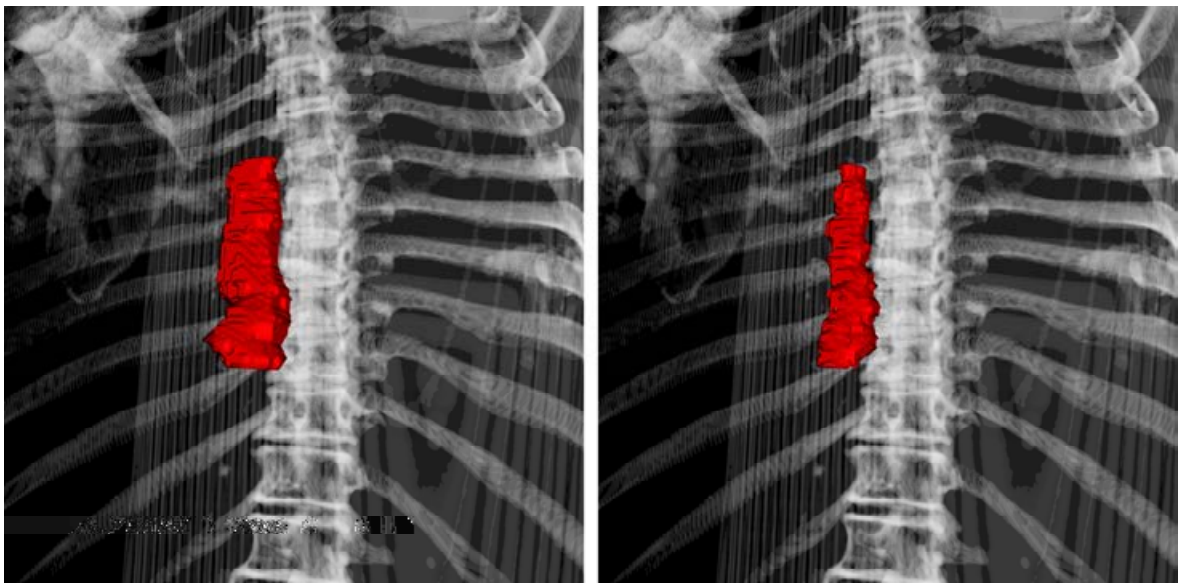

Figure 14 *3D visualization of segmented adenocarcinoma esophageal tumor neoadjuvant pathological stage ypT3N1 from a 64-year old male on CT images (left) and on CT images with aid of PET image data (right), illustrating the resulting volume difference after tumor segmentation.*

5.5 Study IV – Variation in textural analysis parameters during contrast injection of HCC

The observed variation in textural parameters during contrast injection in this study was smaller for each lesion (ie. intra-lesion variability) than the variation was between the corresponding individual average of that texture parameter for all lesions (i.e. inter-lesion variation). Normal hepatic tissue showed the opposite; there was a greater variation in textural parameters over time when compared to the variation between the average value of that texture parameter between individuals. There was no significant drift of texture parameters over time after contrast injection, neither in lesions nor in normal hepatic tissue. The average value of the textural parameters for each analyzed ROI in normal hepatic tissue or lesion over all time points was several factors higher than the resulting slope coefficient of linear regression of textural parameters over time.

In contrast to the observed difference in textural parameters between native and contrast-enhanced CT in study III, no such difference could be observed in this study. This could be due to the lower contrast media dose (50 ml versus approx. 90 ml) but it may also be dependent on tumor type. In HCC the normal dual supply from portal and arterial blood inflow is replaced by a single supply of only arterial inflow. This should result in more apparent changes of textural parameters during the arterial phase of the contrast injection. However, somewhat surprisingly, no such variation was observed at all. However, there were differences between normal hepatic tissue and lesions in the variability and variation of the texture parameters and in the average values of the textural parameters, but those were relatively constant despite contrast media injection. This indicates that there are differences in tumor texture that are not visible to the naked eye prior to contrast media injection. It is tempting to speculate that texture analysis could make contrast media injection redundant in the future, but currently, the differences between tumors and normal hepatic tissue are too small to allow such analyses.

The observed levels of heterogeneity in lesions in comparison to normal tissue in this study were both higher and lower, depending on which textural parameter analyzed. The parameters Energy and Entropy both indicate a lower heterogeneity, while the parameter Inertia indicates a higher heterogeneity. This could reflect differences in contrast uptake due to differences in blood supply, as a single source of blood supply could result in less uneven uptake and wash out in comparison to a dual blood supply. Previously published studies by other research groups have shown an increase of heterogeneity in lesions in comparison to normal hepatic tissue (50,51,91,92). In contrast to those studies, the textural parameters in the current study were calculated as an average over the entire time series rather than from a single time point. The effects of contrast medium uptake and wash out could theoretically make the results not directly comparable to the earlier studies, but as mentioned earlier no effect over time on textural parameters was observed after contrast media injection. Excluding Energy, none of the textural parameters changed more than 1.96 times the SD of the intra-tissue variation, i.e. the observed difference in textural parameters between normal hepatic tissue and lesions were within the 95% confidence interval. This means that the

currently studied textural parameters are not sufficient for making the diagnosis of HCC when used alone. Combinations with other kinds of texture or radiomic parameters could be useful after thorough research.

The same PCT machine with the same imaging settings was used for all included patients, which eliminated differences in textural parameters due to scanner variation. The PCT scans in this study were obtained at a lower tube voltage and with lower flux (mAs, radiation dosage) for each scan cycle when compared to routine contrast-enhanced CT scans. The resulting higher image noise could potentially mask the minute differences caused by contrast enhancement and amplify the observed variation. Also, the lower dosage of contrast medium for PCT scans could result in less contrast enhancement and bin areas into a lower GLCM gray level when rescaling the Hounsfield unit information. This could cause an increase in observed heterogeneity when compared to examinations using standard contrast medium dosage. This might be overcome by fusing images obtained at different time points (120).

The observed drift in textural parameters after contrast injection was so low that precise timing of image acquisition during contrast injection should not be an issue in future studies of HCC. However, the observed seemingly random variation in textural parameters during scanning suggests that there is intrinsic variation between repeated scans. The addition of contrast medium could potentially have increased this variation, but no linear relationship between textural parameters and time after injection was observed. This has to be taken into consideration at statistical analysis of differences between textural parameters in different tissues. In comparison to similar studies of variations in textural parameters at repeated scans after contrast media injection in colorectal cancer (121) and lung cancer (122,123), this study has considerably more time points and is the first study to evaluate the variation during contrast injection in HCC.

The use of only a single 2D slice at texture analysis was a limitation of this study. The number of included voxels for analysis was thereby much smaller than that at the 3D volumetric approach used for study I and III. However, the considerably higher number of images analyzed in this study would have made the 3D approach excessively time-consuming. The use of a single observer for ROI placement was another limitation. However, by limiting the analysis to a single 2D slice and using a highly experienced radiologist the risk of segmentation error should be limited. Variation in ROI placement was probably also reduced by copying the placement of the ROI in the optimum phase in each patient and then pasting it to all the other time points.

6 CONCLUSIONS

This thesis shows that histopathological differences in tumors can be observed using non-invasive diagnostic imaging through textural analysis. The method is applicable to both CT and MRI and on different types of tumors. However, the number of patients included in the study cohorts did not provide sufficient statistical power to enable evaluation of the relationship between textural parameters and overall survival.

Specific conclusions for each of the included studies:

Study I: The GLCM textural parameter Homogeneity can be used to predict *IDH* mutation status for low-grade glioma.

Study II: Semiautomatic segmentation reduces intra- and interobserver variation at CT volumetry of esophageal tumors, compared to manual segmentation. The use of semiautomatic segmentation can also reduce the effect of differing skill levels between the observers.

Study III: Textural analysis can be used to predict ypT-status of post-neoadjuvant esophageal adenocarcinoma. The significant differences in textural parameters observed between esophageal adenocarcinoma and squamous cell carcinoma suggest that the two tumor types should be analyzed separately in future studies involving textural analysis of esophageal cancer.

As the textural parameters of both the remaining tumor volume and the excluded tumor volume after PET guidance are similar, there is no observable difference in tissue type between the volumes. Thus, the addition of PET image data during CT segmentation of esophageal tumors does not improve the correlation between the included textural parameters and ypT-status or overall survival.

Study IV: No additional variation in textural parameters due to use of contrast media for normal hepatic tissue or hepatic lesions was observed, implying that reproducible contrast medium timing should not be an issue at PCT texture analysis of HCC.

7 FUTURE CONSIDERATIONS

Several areas remain for further study regarding the use of textural analysis as a prognostic tool. Although implementing tools to measure textural parameters is relatively simple and can be applied for most imaging modalities, there are still several challenges remaining until these methods can be used reliably in clinical practice.

The results of this thesis show that textural analysis can be used on CT images for differentiation of ypT-status for esophageal adenocarcinoma and separation of adenocarcinoma and squamous cell carcinoma for esophageal cancer. Also, differences in *IDH*-mutation status for low-grade gliomas from MRI images could be detected. Textural analysis has also been shown in other studies to have prognostic value when applied to other types of cancers and imaging modalities. This shows a wide scope of applications of textural analysis as a prognostic tool for different types of cancers and different imaging modalities. Further studies could yield more specific prognostic applications of textural analysis in the treatment of cancer.

Although there have been some studies regarding the variation of textural parameters due to differing imaging equipment and different imaging parameters (98,99), the magnitude of effects on resulting textural parameters needs further research. The assessment of imaging parameters affecting the textural parameters and the quantification of their influence on the variation could be useful for the development of correction methods to reduce those effects, which would be of great importance for multicenter studies using textural parameters to predict treatment effect or survival.

The segmentation of tumor volumes was done using a semiautomated method. The recent development of automated segmentation techniques could lead to improvements in robustness and reduction of interobserver variance (68). Reducing the need for manual user input in the workflow is also of importance in the development of computer-aided diagnosis through machine learning or AI.

There have been several suggestions for the causes of the observed differences in textural parameters between normal tissue and malignant tissue. However, there are only a few studies of the relationship between histopathological samples and textural parameters (60,80). Further exploration of the relationships between histopathological appearance and observed textural parameters might yield additional insight into which specific biological processes in tumor development and tumor treatment response that are observable using textural parameters.

In conclusion, there are several options for further research based on the findings in this thesis.

8 ACKNOWLEDGMENTS

Torkel B. Brismar, my supervisor, for the unwavering belief in the success of this project and support in making it become reality. I hope my variation in productive output has not been a source of too much frustration. Also, for taking care of all expected and unexpected challenges that occurred in the process. The entire process would have been much more frustrating and probably would take at least twice as long without your crucial problem-solving abilities along the way. Finally for correcting all the instances when I mix up singular and plural verb-forms and correcting the times I use “of” instead of “in”.

Ioannis Rouvelas, my co-supervisor, for all the support during my clinical time at Upper Abdominal Surgery and for providing clinical aspects of esophageal cancer. Although I never really learned how to party, we still had a good time.

Gunnar Herlin, for doing the majority of the volume and lesion segmentation. This project would not have been possible without all your work.

Peter Aspelin, for once giving me the opportunity to participate in radiological research by convincing Torkel to take care of me. None of this would have happened otherwise.

Lars Lundell and **Magnus Nilsson**, for providing insightful comments regarding the manuscript we co-authored and for providing access to the NeoRes-data which have been central in this project.

All co-authors, **Asgeir Store Jakola, Anne J.Skjulsvik, Ole Solheim, Hans Kristian Bø, Erik Magnus Berntsen, Ingerid Reinertsen, Sasha Gulati, Petter Förander, Michael A Fischer, Henrik Lehmann, Åse Johnsson, Katarina Brehmer, Anders Svensson**, and **Per Stål.** Thanks for all your contributions and support.

Helena Forssell, Maria Staiger and **Anitta Avesani**, for all administrative help during the project.

My parents **Lian Zhang** and **Xiu-Yun Wang**, for their support during the entire process. My dear grandfather, professor **Xie-Hua Wang**, for his help and guidance. My uncle and aunt, Sir **Bin-Jun Zhuang** and **Ning Zhang** for their care.

My friends, who patiently listened to all of my unsolicited sharing of observations about being a Ph.D. student and put up with it. You also put up with my constant memeing and trolling, which is more than anyone could ask for.

9 REFERENCES

1. Schiff D. Low-grade Gliomas: CONTINUUM: Lifelong Learning in Neurology. 2017 Dec;23(6):1564–79.

2. Forst DA, Nahed BV, Loeffler JS, Batchelor TT. Low-Grade Gliomas. Oncologist. 2014 Apr;19(4):403–13.

3. Pouratian N, Asthagiri A, Jagannathan J, Shaffrey ME, Schiff D. Surgery Insight: the role of surgery in the management of low-grade gliomas. Nat Clin Pract Neurol. 2007 Nov;3(11):628–39.

4. Weller M, van den Bent M, Tonn JC, Stupp R, Preusser M, Cohen-Jonathan-Moyal E, et al. European Association for Neuro-Oncology (EANO) guideline on the diagnosis and treatment of adult astrocytic and oligodendroglial gliomas. The Lancet Oncology. 2017 Jun 1;18(6):e315–29.

5. Louis DN, Perry A, Reifenberger G, von Deimling A, Figarella-Branger D, Cavenee WK, et al. The 2016 World Health Organization Classification of Tumors of the Central Nervous System: a summary. Acta Neuropathol. 2016 Jun 1;131(6):803–20.

6. Cancer Genome Atlas Research Network, Brat DJ, Verhaak RGW, Aldape KD, Yung WKA, Salama SR, et al. Comprehensive, Integrative Genomic Analysis of Diffuse Lower-Grade Gliomas. N Engl J Med. 2015 Jun 25;372(26):2481–98.

7. Wijnenga MMJ, Mattni T, French PJ, Rutten G-J, Leenstra S, Kloet F, et al. Does early resection of presumed low-grade glioma improve survival? A clinical perspective. J Neurooncol. 2017;133(1):137–46.

8. van den Bent MJ, Afra D, de Witte O, Ben Hassel M, Schraub S, Hoang-Xuan K, et al. Long-term efficacy of early versus delayed radiotherapy for low-grade astrocytoma and oligodendroglioma in adults: the EORTC 22845 randomised trial. Lancet. 2005 Sep 17;366(9490):985–90.

9. Shaw EG, Wang M, Coons SW, Brachman DG, Buckner JC, Stelzer KJ, et al. Randomized trial of radiation therapy plus procarbazine, lomustine, and vincristine chemotherapy for supratentorial adult low-grade glioma: initial results of RTOG 9802. J Clin Oncol. 2012 Sep 1;30(25):3065–70.

10. Fisher BJ, Hu C, Macdonald DR, Lesser GJ, Coons SW, Brachman DG, et al. Phase 2 Study of Temozolomide-based Chemoradiation Therapy for High-risk Low-grade Gliomas: Preliminary Results of Radiation Therapy Oncology Group 0424. Int J Radiat Oncol Biol Phys. 2015 Mar 1;91(3):497–504.

11. Radiation Therapy With or Without Temozolomide in Treating Patients With Low-Grade Glioma - Full Text View - ClinicalTrials.gov [Internet]. [cited 2018 Oct 28]. Available from: https://clinicaltrials.gov/ct2/show/NCT00978458

12. Fouke SJ, Benzinger T, Gibson D, Ryken TC, Kalkanis SN, Olson JJ. The role of imaging in the management of adults with diffuse low grade glioma: A systematic review and evidence-based clinical practice guideline. J Neurooncol. 2015 Dec;125(3):457–79.

13. Pirzkall A, Nelson SJ, McKnight TR, Takahashi MM, Li X, Graves EE, et al. Metabolic imaging of low-grade gliomas with three-dimensional magnetic resonance spectroscopy. Int J Radiat Oncol Biol Phys. 2002 Aug 1;53(5):1254–64.

14. Bulik M, Jancalek R, Vanicek J, Skoch A, Mechl M. Potential of MR spectroscopy for assessment of glioma grading. Clin Neurol Neurosurg. 2013 Feb;115(2):146–53.

15. Parent EE, Benayoun M, Ibeanu I, Olson JJ, Hadjipanayis CG, Brat DJ, et al. [18F]Fluciclovine PET discrimination between high- and low-grade gliomas. EJNMMI Res. 2018 Jul 25;8(1):67.

16. Suchorska B, Unterrainer M, Biczok A, Sosnova M, Forbrig R, Bartenstein P, et al. 18F-FET-PET as a biomarker for therapy response in non-contrast enhancing glioma following chemotherapy. J Neurooncol. 2018 Sep;139(3):721–30.

17. Guillevin R, Menuel C, Taillibert S, Capelle L, Costalat R, Abud L, et al. Predicting the outcome of grade II glioma treated with temozolomide using proton magnetic resonance spectroscopy. Br J Cancer. 2011 Jun 7;104(12):1854–61.

18. van den Bent MJ, Wefel JS, Schiff D, Taphoorn MJB, Jaeckle K, Junck L, et al. Response assessment in neuro-oncology (a report of the RANO group): assessment of outcome in trials of diffuse low-grade gliomas. Lancet Oncol. 2011 Jun;12(6):583–93.

19. Short MW, Burgers KG, Fry VT. Esophageal Cancer. Am Fam Physician. 2017 Jan 1;95(1):22–8.

20. Vallböhmer D, Brabender J, Grimminger P, Schröder W, Hölscher AH. Predicting response to neoadjuvant therapy in esophageal cancer. Expert Rev Anticancer Ther. 2011 Sep;11(9):1449–55.

21. Rouvelas I, Zeng W, Lindblad M, Viklund P, Ye W, Lagergren J. Survival after surgery for oesophageal cancer: a population-based study. Lancet Oncol. 2005 Nov;6(11):864–70.

22. Verheij M, Jansen EP, Cats A, van Grieken NCT, Aaronson NK, Boot H, et al. A multicenter randomized phase III trial of neo-adjuvant chemotherapy followed by surgery and chemotherapy or by surgery and chemoradiotherapy in resectable gastric cancer: First results from the CRITICS study. JCO. 2016 May 20;34(15_suppl):4000–4000.

23. Falk J, Carstens H, Lundell L, Albertsson M. Incidence of carcinoma of the oesophagus and gastric cardia. Changes over time and geographical differences. Acta Oncol. 2007;46(8):1070–4.

24. Devesa SS, Blot WJ, Fraumeni JF. Changing patterns in the incidence of esophageal and gastric carcinoma in the United States. Cancer. 1998 Nov 15;83(10):2049–53.

25. Daly JM, Fry WA, Little AG, Winchester DP, McKee RF, Stewart AK, et al. Esophageal cancer: results of an American College of Surgeons Patient Care Evaluation Study. J Am Coll Surg. 2000 May;190(5):562–72; discussion 572-573.

26. Lordick F, Ott K, Krause B-J, Weber WA, Becker K, Stein HJ, et al. PET to assess early metabolic response and to guide treatment of adenocarcinoma of the

oesophagogastric junction: the MUNICON phase II trial. Lancet Oncol. 2007 Sep;8(9):797–805.

27. Klevebro F, Ekman S, Nilsson M. Current trends in multimodality treatment of esophageal and gastroesophageal junction cancer - Review article. Surg Oncol. 2017 Sep;26(3):290–5.

28. Chirieac LR, Swisher SG, Ajani JA, Komaki RR, Correa AM, Morris JS, et al. Posttherapy pathologic stage predicts survival in patients with esophageal carcinoma receiving preoperative chemoradiation. Cancer. 2005 Apr 1;103(7):1347–55.

29. van Rossum PSN, Goense L, Meziani J, Reitsma JB, Siersema PD, Vleggaar FP, et al. Endoscopic biopsy and EUS for the detection of pathologic complete response after neoadjuvant chemoradiotherapy in esophageal cancer: a systematic review and meta-analysis. Gastrointest Endosc. 2016 May;83(5):866–79.

30. Kelley ST, Coppola D, Karl RC. Neoadjuvant chemoradiotherapy is not associated with a higher complication rate vs. surgery alone in patients undergoing esophagectomy. J Gastrointest Surg. 2004 Apr;8(3):227–31; discussion 231-232.

31. van Heijl M, Phoa SSKS, van Berge Henegouwen MI, Omloo JMT, Mearadji BM, Sloof GW, et al. Accuracy and reproducibility of 3D-CT measurements for early response assessment of chemoradiotherapy in patients with oesophageal cancer. Eur J Surg Oncol. 2011 Dec;37(12):1064–71.

32. You JJ, Wong RKS, Darling G, Gulenchyn K, Urbain J-L, Evans WK. Clinical Utility of 18F-Fluorodeoxyglucose Positron Emission Tomography/Computed Tomography in the Staging of Patients with Potentially Resectable Esophageal Cancer. J Thorac Oncol. 2013 Dec;8(12):1563–9.

33. Cervino AR, Pomerri F, Alfieri R, Sileni VC, Castoro C, Galuppo S, et al. 18F-fluorodeoxyglucose PET/computed tomography and risk stratification after neoadjuvant treatment in esophageal cancer patients. Nucl Med Commun. 2014 Feb;35(2):160–8.

34. Wallace MC, Preen D, Jeffrey GP, Adams LA. The evolving epidemiology of hepatocellular carcinoma: a global perspective. Expert Rev Gastroenterol Hepatol. 2015 Jun;9(6):765–79.

35. Balogh J, Victor D, Asham EH, Burroughs SG, Boktour M, Saharia A, et al. Hepatocellular carcinoma: a review. J Hepatocell Carcinoma. 2016 Oct 5;3:41–53.

36. Di Bisceglie AM. Epidemiology and Clinical Presentation of Hepatocellular Carcinoma. Journal of Vascular and Interventional Radiology. 2002 Sep 1;13(9, Part 2):S169–71.

37. Zhang B-H, Yang B-H, Tang Z-Y. Randomized controlled trial of screening for hepatocellular carcinoma. J Cancer Res Clin Oncol. 2004 Jul;130(7):417–22.

38. van Meer S, de Man RA, Coenraad MJ, Sprengers D, van Nieuwkerk KMJ, Klümpen H-J, et al. Surveillance for hepatocellular carcinoma is associated with increased survival: Results from a large cohort in the Netherlands. J Hepatol. 2015 Nov;63(5):1156–63.

39. Song P, Cai Y, Tang H, Li C, Huang J. The clinical management of hepatocellular carcinoma worldwide: A concise review and comparison of current guidelines from 2001 to 2017. Biosci Trends. 2017;11(4):389–98.

40. European Association For The Study Of The Liver, European Organisation For Research And Treatment Of Cancer. EASL-EORTC clinical practice guidelines: management of hepatocellular carcinoma. J Hepatol. 2012 Apr;56(4):908–43.

41. Llovet JM, Brú C, Bruix J. Prognosis of hepatocellular carcinoma: the BCLC staging classification. Semin Liver Dis. 1999;19(3):329–38.

42. Child C, Turcotte J. Surgery and portal hypertension. The liver and portal hypertension. Volume 1 of Major problems in clinical surgery. 1964;

43. Pugh RN, Murray-Lyon IM, Dawson JL, Pietroni MC, Williams R. Transection of the oesophagus for bleeding oesophageal varices. Br J Surg. 1973 Aug;60(8):646–9.

44. Cooper GS, Bellamy P, Dawson NV, Desbiens N, Fulkerson WJ, Goldman L, et al. A prognostic model for patients with end-stage liver disease. Gastroenterology. 1997 Oct;113(4):1278–88.

45. Raza A, Sood GK. Hepatocellular carcinoma review: Current treatment, and evidence-based medicine. World J Gastroenterol. 2014 Apr 21;20(15):4115–27.

46. Sanyal A, Poklepovic A, Moyneur E, Barghout V. Population-based risk factors and resource utilization for HCC: US perspective. Curr Med Res Opin. 2010 Sep;26(9):2183–91.

47. Lee YJ, Lee JM, Lee JS, Lee HY, Park BH, Kim YH, et al. Hepatocellular carcinoma: diagnostic performance of multidetector CT and MR imaging-a systematic review and meta-analysis. Radiology. 2015 Apr;275(1):97–109.

48. Sangiovanni A, Manini MA, Iavarone M, Romeo R, Forzenigo LV, Fraquelli M, et al. The diagnostic and economic impact of contrast imaging techniques in the diagnosis of small hepatocellular carcinoma in cirrhosis. Gut. 2010 May;59(5):638–44.

49. Limkin EJ, Sun R, Dercle L, Zacharaki EI, Robert C, Reuzé S, et al. Promises and challenges for the implementation of computational medical imaging (radiomics) in oncology. Ann Oncol. 2017 Jun 1;28(6):1191–206.

50. Ganeshan B, Miles KA, Young RCD, Chatwin CR. Hepatic enhancement in colorectal cancer: texture analysis correlates with hepatic hemodynamics and patient survival. Acad Radiol. 2007 Dec;14(12):1520–30.

51. Ganeshan B, Miles KA, Young RCD, Chatwin CR. Hepatic entropy and uniformity: additional parameters that can potentially increase the effectiveness of contrast enhancement during abdominal CT. Clin Radiol. 2007 Aug;62(8):761–8.

52. Alic L, Niessen WJ, Veenland JF. Quantification of heterogeneity as a biomarker in tumor imaging: a systematic review. PLoS ONE. 2014;9(10):e110300.

53. Sah B-R, Owczarczyk K, Siddique M, Cook GJR, Goh V. Radiomics in esophageal and gastric cancer. Abdom Radiol [Internet]. 2018 Aug 16 [cited 2018 Nov 1]; Available from: https://doi.org/10.1007/s00261-018-1724-8

54. Bayanati H, E Thornhill R, Souza CA, Sethi-Virmani V, Gupta A, Maziak D, et al. Quantitative CT texture and shape analysis: Can it differentiate benign and malignant mediastinal lymph nodes in patients with primary lung cancer? Eur Radiol. 2015 Feb;25(2):480–7.

55. Yip C, Landau D, Kozarski R, Ganeshan B, Thomas R, Michaelidou A, et al. Primary esophageal cancer: heterogeneity as potential prognostic biomarker in patients treated with definitive chemotherapy and radiation therapy. Radiology. 2014 Jan;270(1):141–8.

56. Yip C, Davnall F, Kozarski R, Landau DB, Cook GJR, Ross P, et al. Assessment of changes in tumor heterogeneity following neoadjuvant chemotherapy in primary esophageal cancer. Dis Esophagus. 2014 Jan 27;

57. Ganeshan B, Skogen K, Pressney I, Coutroubis D, Miles K. Tumour heterogeneity in oesophageal cancer assessed by CT texture analysis: preliminary evidence of an association with tumour metabolism, stage, and survival. Clin Radiol. 2012 Feb;67(2):157–64.

58. Wibmer A, Hricak H, Gondo T, Matsumoto K, Veeraraghavan H, Fehr D, et al. Haralick texture analysis of prostate MRI: utility for differentiating non-cancerous prostate from prostate cancer and differentiating prostate cancers with different Gleason scores. Eur Radiol. 2015 Oct 1;25(10):2840–50.

59. Foley KG, Hills RK, Berthon B, Marshall C, Parkinson C, Lewis WG, et al. Development and validation of a prognostic model incorporating texture analysis derived from standardised segmentation of PET in patients with oesophageal cancer. Eur Radiol. 2018 Jan;28(1):428–36.

60. Ganeshan B, Goh V, Mandeville HC, Ng QS, Hoskin PJ, Miles KA. Non-small cell lung cancer: histopathologic correlates for texture parameters at CT. Radiology. 2013 Jan;266(1):326–36.

61. Diehn M, Nardini C, Wang DS, McGovern S, Jayaraman M, Liang Y, et al. Identification of noninvasive imaging surrogates for brain tumor gene-expression modules. Proc Natl Acad Sci USA. 2008 Apr 1;105(13):5213–8.

62. Zhao S, Kuge Y, Mochizuki T, Takahashi T, Nakada K, Sato M, et al. Biologic correlates of intratumoral heterogeneity in 18F-FDG distribution with regional expression of glucose transporters and hexokinase-II in experimental tumor. J Nucl Med. 2005 Apr;46(4):675–82.

63. Pugachev A, Ruan S, Carlin S, Larson SM, Campa J, Ling CC, et al. Dependence of FDG uptake on tumor microenvironment. Int J Radiat Oncol Biol Phys. 2005 Jun 1;62(2):545–53.

64. Hermans R, Feron M, Bellon E, Dupont P, Van den Bogaert W, Baert AL. Laryngeal tumor volume measurements determined with CT: a study on intra- and interobserver variability. Int J Radiat Oncol Biol Phys. 1998 Feb 1;40(3):553–7.

65. Joskowicz L, Cohen D, Caplan N, Sosna J. Inter-observer variability of manual contour delineation of structures in CT. Eur Radiol. 2018 Sep 7;

66. Filippi M, Horsfield MA, Bressi S, Martinelli V, Baratti C, Reganati P, et al. Intra- and inter-observer agreement of brain MRI lesion volume measurements in multiple sclerosis. A comparison of techniques. Brain. 1995 Dec;118 (Pt 6):1593–600.

67. Parmar C, Velazquez ER, Leijenaar R, Jermoumi M, Carvalho S, Mak RH, et al. Robust Radiomics Feature Quantification Using Semiautomatic Volumetric Segmentation. PLOS ONE. 2014 Jul 15;9(7):e102107.

68. MacKeith SAC, Das T, Graves M, Patterson A, Donnelly N, Mannion R, et al. A Comparison of Repeatability and Usability of Semi-Automated Volume Segmentation Tools for Measurement of Vestibular Schwannomas. Otol Neurotol. 2018 Jul;39(6):e496–505.

69. Berthon B, Marshall C, Evans M, Spezi E. ATLAAS: an automatic decision tree-based learning algorithm for advanced image segmentation in positron emission tomography. Phys Med Biol. 2016 07;61(13):4855–69.

70. Fan Y, Beare R, Matthews H, Schneider P, Kilpatrick N, Clement J, et al. Marker-based watershed transform method for fully automatic mandibular segmentation from CBCT images. Dentomaxillofac Radiol. 2018 Oct 31;20180261.

71. Amiri S, Movahedi MM, Kazemi K, Parsaei H. An Automated MR Image Segmentation System Using Multi-layer Perceptron Neural Network. J Biomed Phys Eng. 2013 Dec;3(4):115–22.

72. Zareie M, Parsaei H, Amiri S, Awan MS, Ghofrani M. Automatic segmentation of vertebrae in 3D CT images using adaptive fast 3D pulse coupled neural networks. Australas Phys Eng Sci Med. 2018 Oct 30;

73. Haralick RM. Statistical and structural approaches to texture. Proceedings of the IEEE. 1979 May;67(5):786–804.

74. Hall-Beyer M. GLCM Texture: A Tutorial v. 3.0 March 2017. 2017 Mar [cited 2018 Nov 2]; Available from: https://prism.ucalgary.ca/handle/1880/51900

75. Conners RW, Trivedi MM, Harlow CA. Segmentation of a high-resolution urban scene using texture operators. Computer vision, graphics, and image processing. 1984;25(3):273–310.

76. Lopes R, Betrouni N. Fractal and multifractal analysis: A review. Medical Image Analysis. 2009 Aug;13(4):634–49.

77. Costa AF, Humpire-Mamani G, Traina AJM. An Efficient Algorithm for Fractal Analysis of Textures. In: 2012 25th SIBGRAPI Conference on Graphics, Patterns and Images. 2012. p. 39–46.

78. Zheng Y, Englander S, Baloch S, Zacharaki EI, Fan Y, Schnall MD, et al. STEP: Spatiotemporal enhancement pattern for MR-based breast tumor diagnosis. Med Phys. 2009 Jul;36(7):3192–204.

79. Skogen K, Schulz A, Helseth E, Ganeshan B, Dormagen JB, Server A. Texture analysis on diffusion tensor imaging: discriminating glioblastoma from single brain metastasis. Acta Radiol. 2018 Jun 3;0284185118780889.

80. Dang M, Lysack JT, Wu T, Matthews TW, Chandarana SP, Brockton NT, et al. MRI texture analysis predicts p53 status in head and neck squamous cell carcinoma. AJNR Am J Neuroradiol. 2015 Jan;36(1):166–70.

81. Ellingson BM, Malkin MG, Rand SD, LaViolette PS, Connelly JM, Mueller WM, et al. Volumetric analysis of functional diffusion maps is a predictive imaging biomarker for cytotoxic and anti-angiogenic treatments in malignant gliomas. J Neurooncol. 2011 Mar 1;102(1):95–103.

82. Zacharaki EI, Morita N, Bhatt P, O'Rourke DM, Melhem ER, Davatzikos C. Survival Analysis of Patients with High-Grade Gliomas Based on Data Mining of Imaging Variables. American Journal of Neuroradiology. 2012 Jun 1;33(6):1065–71.

83. Emblem KE, Pinho MC, Zöllner FG, Due-Tonnessen P, Hald JK, Schad LR, et al. A Generic Support Vector Machine Model for Preoperative Glioma Survival Associations. Radiology. 2014 Dec 8;275(1):228–34.

84. Macyszyn L, Akbari H, Pisapia JM, Da X, Attiah M, Pigrish V, et al. Imaging patterns predict patient survival and molecular subtype in glioblastoma via machine learning techniques. Neuro Oncol. 2015 Jun 20;18(3):417–25.

85. Zhang B, Chang K, Ramkissoon S, Tanguturi S, Bi WL, Reardon DA, et al. Multimodal MRI features predict isocitrate dehydrogenase genotype in high-grade gliomas. Neuro Oncol. 2017 Jan 1;19(1):109–17.

86. Skogen K, Schulz A, Dormagen JB, Ganeshan B, Helseth E, Server A. Diagnostic performance of texture analysis on MRI in grading cerebral gliomas. European Journal of Radiology. 2016 Apr 1;85(4):824–9.

87. Li Z, Wang Y, Yu J, Guo Y, Cao W. Deep Learning based Radiomics (DLR) and its usage in noninvasive IDH1 prediction for low grade glioma. Scientific Reports. 2017 Jul 14;7(1):5467.

88. Tixier F, Le Rest CC, Hatt M, Albarghach N, Pradier O, Metges J-P, et al. Intratumor heterogeneity characterized by textural features on baseline 18F-FDG PET images predicts response to concomitant radiochemotherapy in esophageal cancer. J Nucl Med. 2011 Mar;52(3):369–78.

89. Hatt M, Tixier F, Pierce L, Kinahan PE, Le Rest CC, Visvikis D. Characterization of PET/CT images using texture analysis: the past, the present… any future? Eur J Nucl Med Mol Imaging. 2017 Jan;44(1):151–65.

90. van Rossum PSN, Fried DV, Zhang L, Hofstetter WL, van Vulpen M, Meijer GJ, et al. The Incremental Value of Subjective and Quantitative Assessment of 18F-FDG PET for the Prediction of Pathologic Complete Response to Preoperative Chemoradiotherapy in Esophageal Cancer. J Nucl Med. 2016;57(5):691–700.

91. Brenet Defour L, Mulé S, Tenenhaus A, Piardi T, Sommacale D, Hoeffel C, et al. Hepatocellular carcinoma: CT texture analysis as a predictor of survival after surgical resection. Eur Radiol. 2018 Aug 29;

92. Park HJ, Kim JH, Choi S-Y, Lee ES, Park SJ, Byun JY, et al. Prediction of Therapeutic Response of Hepatocellular Carcinoma to Transcatheter Arterial Chemoembolization

Based on Pretherapeutic Dynamic CT and Textural Findings. AJR Am J Roentgenol. 2017 Oct;209(4):W211–20.

93. Naganawa S, Enooku K, Tateishi R, Akai H, Yasaka K, Shibahara J, et al. Imaging prediction of nonalcoholic steatohepatitis using computed tomography texture analysis. Eur Radiol. 2018 Jul;28(7):3050–8.

94. Bharti P, Mittal D, Ananthasivan R. Characterization of chronic liver disease based on ultrasound images using the variants of grey-level difference matrix. Proc Inst Mech Eng H. 2018 Sep;232(9):884–900.

95. Lubner MG, Jones D, Kloke J, Said A, Pickhardt PJ. CT texture analysis of the liver for assessing hepatic fibrosis in patients with hepatitis C virus. Br J Radiol. 2018 Oct 11;20180153.

96. Mariappan YK, Glaser KJ, Ehman RL. Magnetic resonance elastography: a review. Clin Anat. 2010 Jul;23(5):497–511.

97. Gennisson J-L, Deffieux T, Fink M, Tanter M. Ultrasound elastography: Principles and techniques. Diagnostic and Interventional Imaging. 2013 May 1;94(5):487–95.

98. Mackin D, Fave X, Zhang L, Fried D, Yang J, Taylor B, et al. Measuring Computed Tomography Scanner Variability of Radiomics Features. Investigative Radiology. 2015 Nov;50(11):757.

99. Zhao B, Tan Y, Tsai W-Y, Qi J, Xie C, Lu L, et al. Reproducibility of radiomics for deciphering tumor phenotype with imaging. Scientific Reports. 2016 Mar 24;6:23428.

100. Jakola AS, Skjulsvik AJ, Myrmel KS, Sjåvik K, Unsgård G, Torp SH, et al. Surgical resection versus watchful waiting in low-grade gliomas. Ann Oncol. 2017 Aug 1;28(8):1942–8.

101. Klevebro F, Alexandersson von Döbeln G, Wang N, Johnsen G, Jacobsen A-B, Friesland S, et al. A randomized clinical trial of neoadjuvant chemotherapy versus neoadjuvant chemoradiotherapy for cancer of the oesophagus or gastro-oesophageal junction. Ann Oncol. 2016 Apr;27(4):660–7.

102. Bø HK, Solheim O, Jakola AS, Kvistad K-A, Reinertsen I, Berntsen EM. Intra-rater variability in low-grade glioma segmentation. J Neurooncol. 2017 Jan 1;131(2):393–402.

103. Fedorov A, Beichel R, Kalpathy-Cramer J, Finet J, Fillion-Robin J-C, Pujol S, et al. 3D Slicer as an image computing platform for the Quantitative Imaging Network. Magn Reson Imaging. 2012 Nov;30(9):1323–41.

104. Schneider CA, Rasband WS, Eliceiri KW. NIH Image to ImageJ: 25 years of image analysis. Nat Methods. 2012 Jul;9(7):671–5.

105. Segmentation Editor [Internet]. ImageJ. [cited 2018 Jan 19]. Available from: http://imagej.net/Segmentation_Editor

106. R Core Team. R: A Language and Environment for Statistical Computing [Internet]. Vienna, Austria: R Foundation for Statistical Computing; 2013. Available from: http://www.R-project.org/

107. Bland JM, Altman DG. Statistical methods for assessing agreement between two methods of clinical measurement. Lancet. 1986 Feb 8;1(8476):307–10.

108. Schemper M, Smith TL. A note on quantifying follow-up in studies of failure time. Contemporary Clinical Trials. 1996 Aug 1;17(4):343–6.

109. Chang EF, Smith JS, Chang SM, Lamborn KR, Prados MD, Butowski N, et al. Preoperative prognostic classification system for hemispheric low-grade gliomas in adults. J Neurosurg. 2008 Nov;109(5):817–24.

110. Dercle L, Ammari S, Bateson M, Durand PB, Haspinger E, Massard C, et al. Limits of radiomic-based entropy as a surrogate of tumor heterogeneity: ROI-area, acquisition protocol and tissue site exert substantial influence. Sci Rep. 2017 Aug 11;7(1):7952.

111. Pallud J, Blonski M, Mandonnet E, Audureau E, Fontaine D, Sanai N, et al. Velocity of tumor spontaneous expansion predicts long-term outcomes for diffuse low-grade gliomas. Neuro Oncol. 2013 May 1;15(5):595–606.

112. Tanenbaum LN, Tsiouris AJ, Johnson AN, Naidich TP, DeLano MC, Melhem ER, et al. Synthetic MRI for Clinical Neuroimaging: Results of the Magnetic Resonance Image Compilation (MAGiC) Prospective, Multicenter, Multireader Trial. American Journal of Neuroradiology. 2017 Jun 1;38(6):1103–10.

113. Liang EY, Chan A, Chung SC, Metreweli C. Short communication: oesophageal tumour volume measurement using spiral CT. Br J Radiol. 1996 Apr;69(820):344–7.

114. Griffith JF, Chan AC, Chow LT, Leung SF, Lam YH, Liang EY, et al. Assessing chemotherapy response of squamous cell oesophageal carcinoma with spiral CT. Br J Radiol. 1999 Jul;72(859):678–84.

115. Thomas L, Lapa C, Bundschuh RA, Polat B, Sonke J-J, Guckenberger M. Tumour delineation in oesophageal cancer - A prospective study of delineation in PET and CT with and without endoscopically placed clip markers. Radiother Oncol. 2015 Aug;116(2):269–75.

116. Muijs CT, Beukema JC, Pruim J, Mul VE, Groen H, Plukker JT, et al. A systematic review on the role of FDG-PET/CT in tumour delineation and radiotherapy planning in patients with esophageal cancer. Radiotherapy and Oncology. 2010 Nov 1;97(2):165–71.

117. Kitajima K, Nakajo M, Kaida H, Minamimoto R, Hirata K, Tsurusaki M, et al. Present and future roles of FDG-PET/CT imaging in the management of gastrointestinal cancer: an update. Nagoya J Med Sci. 2017 Nov;79(4):527–43.

118. Rice TW, Ishwaran H, Kelsen DP, Hofstetter WL, Apperson-Hansen C, Blackstone EH. Recommendations for Neoadjuvant Pathologic Staging (ypTNM) of Cancer of the Esophagus and Esophagogastric Junction for the 8th Edition AJCC/UICC Staging Manuals. Dis Esophagus. 2016 Nov;29(8):906–12.

119. Cook GJR, Siddique M, Taylor BP, Yip C, Chicklore S, Goh V. Radiomics in PET: principles and applications. Clin Transl Imaging. 2014 Jun 1;2(3):269–76.

120. Brehmer K, Brismar TB, Morsbach F, Svensson A, Stål P, Tzortzakakis A, et al. Triple Arterial Phase CT of the Liver with Radiation Dose Equivalent to That of Single Arterial Phase CT: Initial Experience. Radiology. 2018 Oct;289(1):111–8.

121. Hu P, Wang J, Zhong H, Zhou Z, Shen L, Hu W, et al. Reproducibility with repeat CT in radiomics study for rectal cancer. Oncotarget. 2016 Nov 1;7(44):71440–6.

122. Balagurunathan Y, Kumar V, Gu Y, Kim J, Wang H, Liu Y, et al. Test–Retest Reproducibility Analysis of Lung CT Image Features. J Digit Imaging. 2014 Dec 1;27(6):805–23.

123. Zhao B, James LP, Moskowitz CS, Guo P, Ginsberg MS, Lefkowitz RA, et al. Evaluating variability in tumor measurements from same-day repeat CT scans of patients with non-small cell lung cancer. Radiology. 2009 Jul;252(1):263–72.